Moisture Sources and Pathways Determine Stable Isotope Signature of Himalayan Waters in Nepal

Hima Hassenruck-Gudipati, Christoff Andermann, Sylvia Dee, Camilla Brunello, Krishna Pyari Baidya, Dirk Sachse, Hanno Meyer, Niels Hovius

AGU Advances

RESEARCH ARTICLE
10.1029/2022AV000735

Moisture Sources and Pathways Determine Stable Isotope Signature of Himalayan Waters in Nepal

Hima J. Hassenruck-Gudipati[1,2,3], Christoff Andermann[1,4], Sylvia Dee[5], Camilla F. Brunello[1,6], Krishna Pyari Baidya[7], Dirk Sachse[1], Hanno Meyer[8], and Niels Hovius[1,9]

[1]Helmholtz Centre Potsdam, GFZ German Research Center for Geosciences, Section 4.6: Geomorphology, Potsdam, Germany, [2]Department of Geological Sciences, Jackson School of Geosciences, University of Texas at Austin, Austin, TX, USA, [3]Department of Earth & Environmental Sciences, University of Minnesota, Minneapolis, MN, USA, [4]Géosciences Rennes, Univ Rennes, CNRS, UMR 6118, Rennes, France, [5]Department of Earth, Environmental, and Planetary Sciences, Rice University, Houston, TX, USA, [6]Alfred Wegener Institute for Polar and Marine Research, Bremerhaven, Germany, [7]Department of Hydrology and Meteorology, Kathmandu, Nepal, [8]Alfred Wegener Institute for Polar and Marine Research, Potsdam, Germany, [9]Institute of Earth and Environmental Sciences, University of Potsdam, Potsdam, Germany

Key Points:

- The isotopic signature of rivers in the central Himalayas is strongly buffered by a well-mixed groundwater reservoir
- Moisture sources and transport processes determine distinct pre-monsoon and monsoon rainfall isotopic signatures in the Himalayas
- Water recycling in the Gangetic plain sets the isotopic composition of pre-monsoon rainfall across the central Himalayan mountain range

Supporting Information:

Supporting Information may be found in the online version of this article.

Correspondence to:

H. J. Hassenruck-Gudipati,
himahg@utexas.edu

Citation:

Hassenruck-Gudipati, H. J., Andermann, C., Dee, S., Brunello, C. F., Baidya, K. P., Sachse, D., et al. (2023). Moisture sources and pathways determine stable isotope signature of Himalayan waters in Nepal. *AGU Advances*, *4*, e2022AV000735. https://doi.org/10.1029/2022AV000735

Received 3 MAY 2021
Accepted 8 NOV 2022

Peer Review The peer review history for this article is available as a PDF in the Supporting Information.

Author Contributions:

Conceptualization: Hima J. Hassenruck-Gudipati, Christoff Andermann, Sylvia Dee, Niels Hovius
Data curation: Hima J. Hassenruck-Gudipati, Christoff Andermann, Dirk Sachse, Hanno Meyer
Formal analysis: Hima J. Hassenruck-Gudipati, Christoff Andermann, Camilla F. Brunello
Funding acquisition: Christoff Andermann, Niels Hovius

Abstract

The Himalayan mountain range produces one of the steepest and largest rainfall gradients on Earth, with >3 m/yr rainfall difference over a ∼100 km distance. The Indian Summer Monsoon (ISM) contributes more than 80% to the annual precipitation budget of the central Himalayas. The remaining 20% falls mainly during pre-ISM season. Understanding the seasonal cycle and the transfer pathways of moisture from precipitation to the rivers is crucial for constraining water availability in a warming climate. However, the partitioning of moisture into the different storage systems such as snow, glacier, and groundwater and their relative contribution to river discharge throughout the year remains under-constrained. Here, we present novel field data from the Kali Gandaki, a trans-Himalayan river, and use 4-year time series of river and rain water stable isotope composition ($\delta^{18}O$ and $\delta^{2}H$ values) as well as river discharge, satellite Global Precipitation Measurement amounts, and moisture source trajectories to constrain hydrological variability. We find that rainfall before the onset of the ISM is isotopically distinct and that ISM rain and groundwater have similar isotopic values. Our study lays the groundwork for using isotopic measurements to track changes in precipitation sources during the pre-ISM to ISM transition in this key region of orographic precipitation. Specifically, we highlight the role of pre-ISM precipitation, derived from the Gangetic plain, to define the seasonal river isotopic variability across the central Himalayas. Lastly, isotopic values across the catchment document the importance of a large well-mixed groundwater reservoir supplying river discharge, especially during the non-ISM season.

Plain Language Summary

Himalayan rivers are the essential water source for downstream communities. However, it is still not well understood where precipitation moisture comes from and how it is transferred to rivers. In particular, the role of intermediate water storage in groundwater, snow, and glacier is not well understood. To resolve these issues, we collected river water, groundwater, snow, glacier, and rain samples across Central Himalayas in Nepal and analyzed their isotopic composition. We determine characteristic signatures of the different moisture sources to trace water transfer in and out of the study area. Combining field observations with satellite observations and numerical models, we show that rainfall before the beginning of the Indian Summer Monsoon undergoes several evaporation-precipitation cycles and is derived from the Gangetic foreland, while monsoon precipitation is derived from the Indian and Arabian Sea. During our 4-year observation period, pre-Monsoon precipitation resulted in the largest variation in river water isotopes. We also identify groundwater as the principal source of river discharge during the dry season. This work highlights the importance of detailed spatiotemporal isotopic analysis to determine precipitation moisture sources, how water sources change throughout the year, and how they contribute to river flow in the central Himalayas.

1. Introduction

Understanding the future of Himalayan water resources relies on the investigation of their pathways and storage on the catchment scale. Rivers draining the Himalayas are fed by water sources that comingle several moisture pathways. These moisture pathways are associated with different seasonal circulation patterns, including the Indian Summer Monsoon (IMS), pre-ISM, and Westerly disturbance-derived moisture (e.g., Brunello

Investigation: Hima J. Hassenruck-Gudipati, Christoff Andermann, Camilla F. Brunello, Krishna Pyari Baidya, Dirk Sachse, Niels Hovius
Methodology: Hima J. Hassenruck-Gudipati, Christoff Andermann, Sylvia Dee, Dirk Sachse, Hanno Meyer
Project Administration: Christoff Andermann
Resources: Christoff Andermann, Hanno Meyer, Niels Hovius
Software: Hima J. Hassenruck-Gudipati, Christoff Andermann, Sylvia Dee
Supervision: Christoff Andermann
Validation: Dirk Sachse, Hanno Meyer
Visualization: Hima J. Hassenruck-Gudipati
Writing – original draft: Hima J. Hassenruck-Gudipati, Christoff Andermann, Sylvia Dee
Writing – review & editing: Hima J. Hassenruck-Gudipati, Christoff Andermann, Sylvia Dee, Camilla F. Brunello, Krishna Pyari Baidya, Dirk Sachse, Niels Hovius

et al., 2020; Galewsky et al., 2016; Yao et al., 2013). Historically, end-member sources of river discharge, such as seasonally varying rain, groundwater springs, snow, and glaciers, have been disentangled through hydrological and modeling studies for large Himalayan catchments (Andermann, Longuevergne, et al., 2012; Bookhagen & Burbank, 2010; Immerzeel et al., 2010; Nepal et al., 2014; Wulf et al., 2016). Recently, groundwater recharge has been shown to occur only after sufficient moisture has accumulated during the pre-monsoon season when the soil is saturated (Illien et al., 2021). However, in situ measurements of river end-member characteristics and data linking the sources of precipitation to river output in this complex setting remain sparse. This critically limits our ability to evaluate the stability of future Himalayan water resources, including groundwater contributions to river discharge.

Stable water isotopes provide a tool for fingerprinting water origin in the landscape in time and space and can facilitate partitioning of each source's contribution to river discharge (Boral et al., 2019). Moreover, scrutinizing temporal and spatial isotopic signals in the hydrosphere provides important insights into interpreting past climate from geological archives, which may be influenced by contributions of water sources from seasons beyond the ISM (Breitenbach et al., 2010; Brunello et al., 2019; Gajurel et al., 2006; Taft et al., 2012; Wolf et al., 2020; Y. Cai et al., 2015). Specifically, different sources of precipitation and river discharge have a distinct stable isotopic signature. This is generally reported as the stable isotope ratio for either oxygen or hydrogen, in delta notation ($\delta^{18}O$ and $\delta^{2}H$) in permille (‰), and represents the deviation from a standard (e.g., Vienna Standard Mean Ocean Water, Sharp, 2017). Isotope ratios are altered via fractionation processes. The two that dominate are equilibrium fractionation (e.g., associated with temperature-dependent condensation of vapor) and kinetic fractionation, (e.g., during evaporation) (Ciais & Jouzel, 1994; Craig & Gordon, 1965; Gat, 1996; Jouzel & Merlivat, 1984; Majoube, 1971). Fractionation processes are temperature and pressure dependent, as such the global observations of precipitation isotopes depict a distinct linear, empirical relationship, called the global meteoric water line (Sharp, 2017). A second-order parameter, deuterium-excess (d-excess $= \delta^{2}H - 8 \times \delta^{18}O$) denotes the relative deviation of $\delta^{18}O$ and $\delta^{2}H$ from this relationship and is traditionally interpreted as a diagnostic for evaporative processes and moisture origin (Sharp, 2017).

Condensation of water vapor and progressive rainout drive decreases in both $\delta^{18}O$ and $\delta^{2}H$ as clouds rise at the orographic barrier. In contrast, moisture recycling in the landscape, by repeated rainout and re-evaporation along a transport path, causes enrichment in heavier surface water isotopes and thus a more positive precipitation isotope signature (Winnick et al., 2014), capable of masking negative trends. One such landscape where convection and re-evaporation are important is the heavily irrigated Gangetic Plain. During the pre-ISM, the surface waters in the regions are strongly enriched in heavier isotopes (Gajurel et al., 2006; Kumar et al., 2019; Mukherjee et al., 2007). While these individual impacts on isotope ratios in local moisture are well-documented, the seasonal overprinting and mixing of isotopic signatures due to the combination of these processes remains difficult to deconvolve. For example, for the adjacent Asian Monsoon region, Z. Cai et al. (2018) showed the effect of convection amount on more positive isotopic signatures from moisture sources such as the Bay of Bengal and the South China Sea.

Previous work shows that, for large parts of the Himalayas, the precipitation delivered by the ISM dominates the annual water budget (Bookhagen & Burbank, 2010; Brunello et al., 2020; Wang et al., 2020; Yao et al., 2013). Extrapolating from rainfall data measured for New Delhi, the isotopic signature of the ISM has a lower (~8‰) d-excess compared to the higher (~22‰) d-excess derived from winter Westerly disturbance-derived moisture (Gat & Carmi, 1970; Karim & Veizer, 2002). Additionally, seasonality of Himalayan river discharge and the timing of the vegetative season are often attributed to the ISM. However, precipitation in other seasons, groundwater, snow, and glacier reservoirs might also play a role in modulating seasonal river discharge.

In the Himalayas, $\delta^{2}H$ and d-excess in rivers have historically been used as indicators of moisture source and paleoelevation (Bershaw et al., 2012; Garzione et al., 2000; Hren et al., 2009; Li & Garzione, 2017; Meese et al., 2018). The Pre-ISM season rain is the most isotopically distinct water source across the central Himalayan orographic barrier, with positive $\delta^{2}H$ values contrasting very negative ISM rain values (Breitenbach et al., 2010; Brunello et al., 2019, 2020; Wolf et al., 2020). However, partitioning the individual water sources to Himalayan rivers with stable isotopes has proven challenging and typically requires additional techniques to differentiate between snow versus glacier melt (e.g., Wilson et al., 2015). Complicating this, recent literature suggests additional seasonal variability in precipitation d-excess values exists outside the range of that expected due to changing moisture pathways, driven by changes in temperature and relative humidity of the source region (Pfahl & Sodemann, 2014).

To resolve these uncertainties, in this study, we present a comprehensive, high-resolution data set of observations from rivers, as well as potential end-members rain, glacier, snow, and groundwater springs (from now on referred to as springs) across the central Himalayas. We investigate how pre-ISM precipitation isotopic signals described above are incorporated into catchment hydrology, and whether these pathways produce a distinguishable isotopic signal. Specifically, our data set facilitates an investigation of whether Gangetic plain evaporation (i.e., continental moisture recycling) is an independent contributor to precipitation in the central Himalayas. Our data and results answer three timely questions surrounding moisture supply in the central Himalayas: (a) how is the isotopic signature of rain routed through the hydrological system? (b) What is the seasonality of precipitation isotopic signature? (c) What is the isotopic recognizable end-member sources for the central Himalayas? The high-resolution data set reveals a well-mixed groundwater isotopic signature. We also show a strong seasonal cycle in river and precipitation stable isotopes. This work provides much needed constraints on precipitation moisture source variability and water supply contribution in the trans-Himalayan Kali Gandaki River catchment.

2. Data and Methods

2.1. Study Area

The Kali Gandaki River, Nepal, cuts through the High Himalayan orographic barrier, funneling water southward from the southern margin of the Tibetan plateau through the Himalayan range, down to the Gangetic plain. The river drains an area of 11,900 km^2, mixing waters originating at different elevations and climate zones. This catchment covers ∼8 km of relief, ranging from a minimum of ∼150 m at the southern mountain front to the high summits of Dhaulagiri and Annapurna (both >8,000 masl.). These mountains built an east-west trending orographic barrier, while the low-lying river valley functions as a natural south to north conduit for air masses across the mountain range (Struck et al., 2015; Talchabhadel et al., 2021; Zängl et al., 2001). North of the orographic barrier, local relief is more subdued, rising more gently to a low-relief drainage divide with the upper Tsangpo River to the north.

The catchment topographic profile is reflected in the strong precipitation gradient, with rainfall rates exceeding 3 m/yr at the Himalayan southern front, and around 0.2 m/yr in the upper Kali Gandaki valley (Figure 1a). Approximately 10% of the drainage area is glaciated (Struck et al., 2015). We define the seasons statistically based on precipitation timeseries, after Brunello et al. (2020), with the ISM commonly starting mid-June and ending in September (Figure 2). The catchment also receives moisture in the pre-ISM season (March to mid-June). There is very little precipitation in post-ISM and winter (October–February). Therefore, we refer to these months as the dry season.

2.2. Hydrometeorological Data Sets: River Discharge and Catchment Precipitation

Kali Gandaki River discharge was measured from January 2014 to December 2017 at two locations (Figure 1). At Lete (28.65°N, 83.59°E), situated at the transition from the upper Tibetan segment into the steeper Himalayan segment (upstream area = 3,463 km^2), river discharge was calculated from stage height readings using a rating curve. Readings do not cover January–June 2014 and April–June 2016 (Figure 2). Near Purtighat (28.05°N, 83.56°E), located at the boundary between the high Himalayas and the frontal ranges (upstream area = 6,922 km^2), river discharge records were obtained from the Mirmi hydropower operator.

Precipitation amounts, both of rain and snow, were derived from the Global Precipitation Measurement (GPM) at 0.1° resolution (Huffman et al., 2019). Snow-rain distinction was obtained from the probability of liquid precipitation band. Two subsections of the study area were investigated: the sub-catchments above Lete and between Lete and Purtighat (3,459 km^2).

2.3. Water Samples

To constrain spatiotemporal water contributions to the Kali Gandaki river, we collected a total of 1,764 samples (Figures 1 and 2, Andermann et al., 2021). Areal samples were repeated throughout the year to constrain the seasonal variability. Moreover, we conducted a daily to weekly sampling of river and rainwater for high-resolution monitoring at Lete and Purtighat. Our sampling location at Purtighat was located 15 km upstream of the Mirmi hydropower station (Figure 1). The data, sampling and analytical procedures are published separately (Andermann et al., 2021).

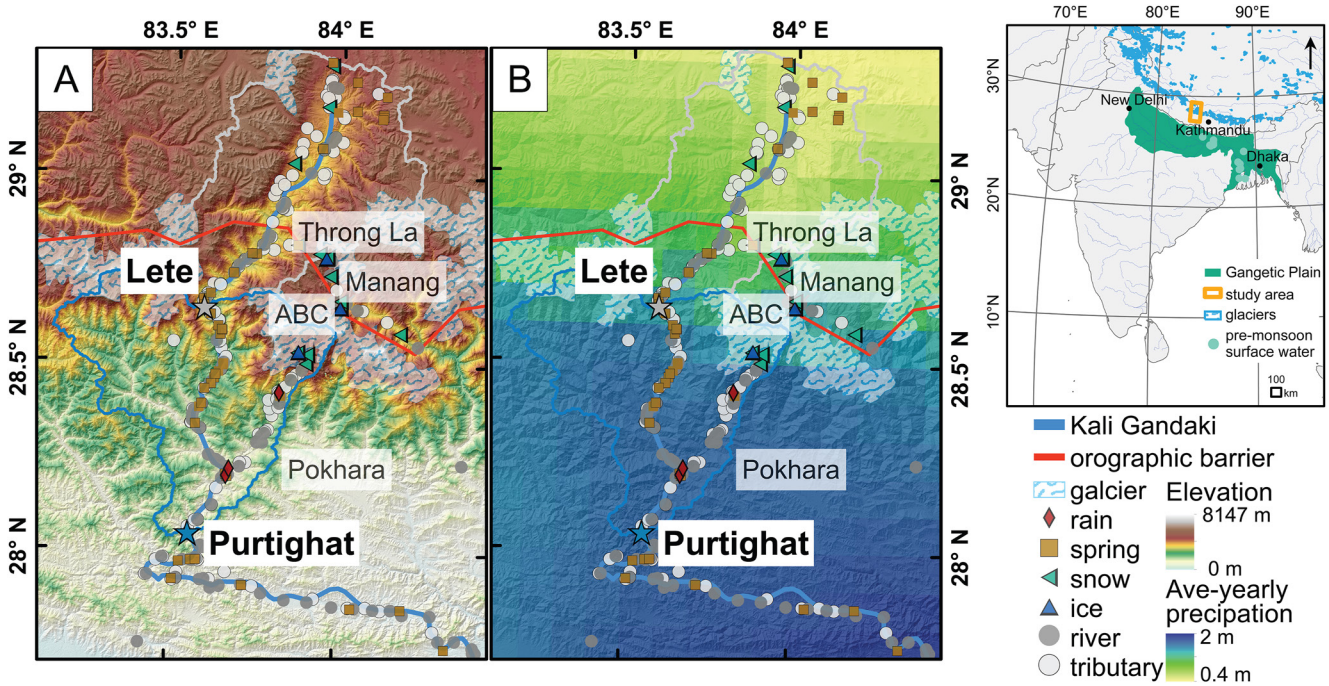

Figure 1. Overview of the Kali Gandaki River catchment with sampling locations. The insert right shows the broader regional context outlining the study area. (a) Elevation overlain on a shaded relief map. (b) Precipitation amount over shaded relief. The gray and blue outline mark Lete and Purtighat sub-catchments, respectively. The red line represents the orographic barrier defined as the 0.5 m/yr isohyete (from Andermann, Crave, et al. (2012)). Precipitation is the yearly mean, based on Global Precipitation Measurement. Sampling locations are marked as dark gray dots for rivers, light gray dots for tributaries, red diamonds for rain, brown squares for groundwater springs including hot springs, light green left-pointing triangles for snow, and blue triangles for glaciers. The gray and blue stars mark the Lete and Purtighat timeseries sampling location. ABC refers to the Annapurna Base Camp and the Gangetic plain extent is taken from Dinerstein et al. (2017).

2.3.1. River End-Members: Rain, Springs, Snow, and Glaciers

To assess potential source contributions to discharge of the Kali Gandaki River, we sampled input end-members with a wide spatial coverage: rain, n = 216; snow, n = 41; glaciers, n = 11; groundwater, n = 64, including hot springs, n = 10. Starting in 2016, rain samples were collected for each rain event throughout the year at Lete (n = 128) at the orographic barrier. Lacking a secure sampling site in the lower Kali Gandaki at Purtighat (28.05°N, 83.56°E, 600 m), we use rain samples from Kathmandu (27.71°N, 85.32°E, 1,300 m, n = 80). We consider these samples as representative of the southern part of the catchment. Groundwater springs were sampled throughout the catchment, covering all major geological units of the catchment. Snow and glacier samples were mostly collected in spring of 2015 around the orographic barrier (Figure 1). To avoid surface alteration, we dug snow pits through the 2–5 uppermost layers of snow and sampled unaltered snow, avoiding the top 2–3 cm of layers. Before the sampling campaign in March 2015 a strong snowfall event happened in the region and most of the snow samples represent fresh snow from this period. Glacier samples were glacier ice grab samples from the ablation zones of glaciers. A total of three glaciers were sampled with several sampled at individual layers (Annapurna Base Camp (debris-covered glacier, n = 1); Manang (clear-ice glacier: n = 5); and Throng La Pass (clear-ice glacier: n = 4)). Snow and glacier samples were melted in plastic bags at ambient temperature and transferred to 30 ml bottles.

2.3.2. River and Tributary Samples

The collected river (n = 1,089) and tributary (n = 160) water samples span the entire latitudinal range across the orographic barrier. River and tributary samples were collected during various field campaigns between 2013 and 2016 and supplemented with published data by Garzione et al. (2000) and Li and Garzione (2017). Timeseries sampling spanned four ISM seasons at Lete (n = 380) and Purtighat (n = 695). At Lete and Purtighat, samples were taken weekly from June 2013 until May 2015 and after that daily (https://doi.org/10.5880/GFZ.4.6.2021.004). From the available time series, samples were analyzed irregularly, with at least one sample per week.

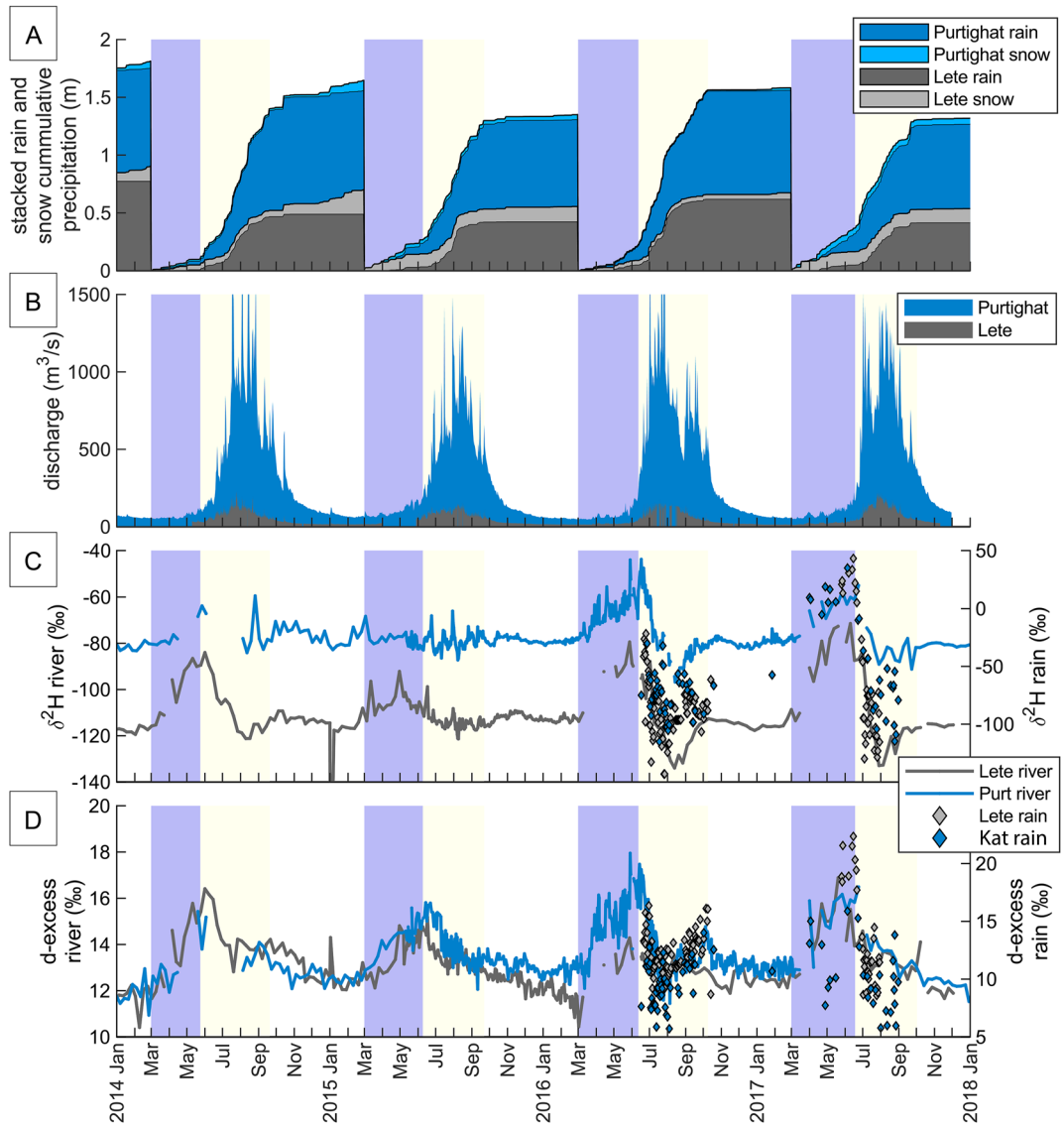

Figure 2. Meteorology and hydrology time series for the two Kali Gandaki River sub-catchments. (a) Global Precipitation Measurement cumulative sum of rain and snow precipitation at Lete (gray) and Purtighat (blue). The lighter color tone indicates the snow amount stacked on top of the darker toned rain. (b) Discharge measured at Lete (gray) and Purtighat (blue). (c) δ^2H river samples for Lete and Purtighat (left *y*-axis). Diamonds are rain samples from Lete (gray) and Kathmandu (blue; both right *y*-axis). The offset between Purtighat and Lete highlights that Lete (gray) is located at a higher elevation further north compared to Purtighat (blue). (d) D-excess river samples for both Lete and Purtighat (left *y*-axis) as well as rain samples (diamonds; right *y*-axis) for Lete and Kathmandu. The seasonal variability in d-excess is greater than the difference between the two locations. Samples for Purtighat in 2014 (n = 28/695) and Lete in 2016 (n = 34/380) have been removed as they may have been susceptible to evaporation post-sampling.

2.4. Precipitation Moisture Trajectories Extraction and Isotope Models

Our extensive sampling is paired with modeling effort to predict the south to north latitudinal trend in precipitation isotopic composition and its seasonality. We do this by (a) considering seasonally varying moisture sources reconstructed by trajectory modeling, and (b) assuming that Rayleigh distillation rainout and rain re-evaporation have a first-order effect on precipitation isotope values. This effect may be captured by single-column Rayleigh isotope distillation modeling.

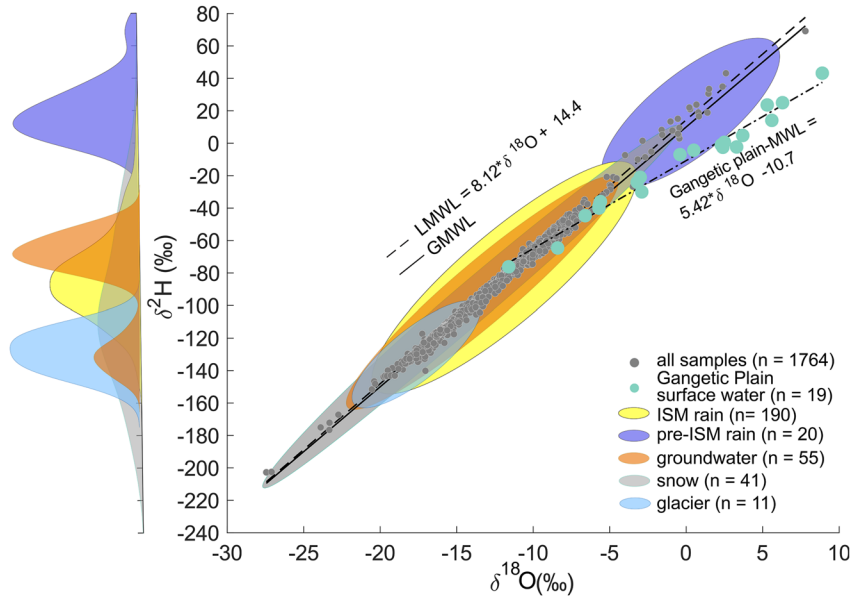

Figure 3. The measured water isotope samples plot along the Global Meteoric Water Line (GMWL; solid; $\delta^2H = 8 \times d^{18}O + 10$). The dashed line is the Local Meteoric Water Line (LMWL; $\delta^2H = 8.12 \times d^{18}O + 14.4$). The doted dashed line ($\delta^2H = 5.42 \times d^{18}O - 10.7$) is the LMWL for surface water values from the Gangetic Plain (green circles; Gajurel et al., 2006; Kumar et al., 2019; Mukherjee et al., 2007). Ellipses are representative of the 95% standard error in their long axis and are exaggerated in their minor axis for visualization. Kernel density plots on the left *y*-axis show the distribution of δ^2H values measured for each end-member. Each end-member has the following sample numbers: Indian Summer Monsoon (ISM) rain ($n = 190$), pre-ISM rain ($n = 20$), groundwater spring ($n = 55$, not including hot springs), snow ($n = 41$), and glacier ($n = 11$). The water samples with the most positive δ^2H and $\delta^{18}O$ values were collected from rain and snow during the pre-monsoon.

2.4.1. Moisture Trajectories

To determine the sources of moisture delivered to the Kali Gandaki catchment, we employed Hybrid Single-Particle Lagrangian Integrated Trajectories (HYSPLIT) modeling (Draxler, 1999; Kalnay et al., 1996; Stein et al., 2015). Trajectories were calculated using the NCAR/NCEP global reanalysis data set and the contributions were assessed from cloud heights of 500–3,000 m, at 500 m intervals, every 6 hr, using the Pysplit package (Cross, 2015; Warner, 2018). Trajectories were run backward for 168 hr for rain events at Lete, over the monitoring period from 2014 to 2017. The seasonal and interannual variability of moisture sourcing were determined using precipitation weighted trajectories for this period (Text S1 in Supporting Information S1).

2.4.2. Single-Column Rayleigh Isotope Distillation Model

To support our empirical analysis and interpretation of the fractionation processes we employed a single-column Rayleigh distillation model, following Rowley et al. (2001), to constrain the physical processes. In this model, moisture is lifted at each elevation step and water vapor saturation, constrained by High Asia Refined data set (Maussion et al., 2011, 2014) for the catchment, determines the amount of condensation removed as rain (Text S2 in Supporting Information S1). With each rainout event, isotope values are determined based on Rayleigh distillation and empirical temperature fractionation curves incorporating both vapor-liquid and vapor-ice fractionation. Initial conditions such as vapor isotope ratios, air temperature, and relative humidity were determined based on the origin of the moisture. For pre-ISM, initial vapor isotopes are determined from a constant evaporation model of surface water isotopes on the Gangetic Plain plotted in (Figure 3) with atmospheric isotopic values derived from precipitation isotopic values (Global Network of Isotopes in Precipitation (GNIP) station New Delhi, India). Temperature and relative humidity at the moisture source are taken from NCEP reanalysis within a bounding box (20.5°N, 76.5°E, 29.5°N, 80.5°E) representing the Gangetic plain. For ISM, vapor isotopes are approximated from GNIP precipitation isotopic values in Dhaka, Bangladesh and climatic parameters within a bounding box (17.1°N, 87.5°E, 21.3°N, 91.9°E) located in the Bay of Bengal (see Text S2 in Supporting Information S1 for details of methodology). The Gangetic plain and the Bay of Bengal are the two investigated moisture sources of pre-ISM and ISM precipitation in the central Himalayas.

3. Results

3.1. Catchment Precipitation

We first report the mean GPM rain and snow for the period 2000–2018, with total precipitation equaling the sum of both. A full list of statistical parameters is reported in Tables S1 and S2 in Supporting Information S1. South of the orographic barrier, rainfall data exhibit a clear seasonal cycle as well as interannual variability (Figure 2). Mean annual rainfall in the southern Purtighat sub-catchment was 1,488 mm, with 1% (19 mm) of the annual total falling in winter, 13% (187 mm) during pre-ISM, 83% (1,230 mm) during ISM, and 3% (52 mm) in the post-ISM period (Table S1 in Supporting Information S1). Winter is defined between 1 December and 1 March. Meanwhile, pre-ISM, ISM, and post-ISM are defined outside of the 1 March to 1 December bound with the statistically defined ISM onset and withdrawal dates (Tables S3 and S4 in Supporting Information S1, Brunello et al., 2020). Year 2014 had weak pre-ISM rainfall with only 138 mm and stronger post-ISM rainfall with 108 mm. Year 2015 had the opposite pattern, with a strong pre-ISM (208 mm) and relatively weak post-ISM (32 mm).

In the northern Lete sub-catchment (see Section 2.2), GPM rainfall data showed a similar seasonal cycle and interannual variability compared to the south, but less than half in magnitude, with an average annual total rainfall of 624 mm. Pre-ISM, ISM, and post-ISM rainfall contributions were 6% (38 mm), 92% (575 mm), and 2% (11 mm), respectively (Table S2 in Supporting Information S1). In 2014, the post-ISM rainfall was 90% above the season mean. Total ISM rain was lower (less than third quantile (2000–2018)) for 2015, while both 2014 and 2016 had relatively high ISM rain and discharge values (Tables S5 and S6 in Supporting Information S1).

In the Purtighat sub-catchment (see Section 2.2), GPM winter and pre-ISM mean seasonal snowfall for the entire period was 32 and 14 mm, respectively. For the Lete sub-catchment, the equivalent values were 37 and 56 mm (Tables S1 and S2 in Supporting Information S1). The period from post-ISM 2014 to pre-ISM 2015 had exceptional snowfall, with a total of 272 mm (2.5-σ above mean) and 100 mm (1.9-σ above mean) for the Lete and Purtighat sub-catchments, respectively, creating a meteorologically unique signal for the period of investigation.

3.2. Precipitation Moisture Source Uptake

Moisture source uptake along trajectories for the 4 years spanning this study (2014–2017) show that precipitation at Lete, at the orographic barrier, was delivered along two principal pathways, one from continental sources during the pre-monsoon and a second during ISM originating from the Bay of Bengal and the Arabian Sea (Figures 4a and 4b). Westerly disturbance-derived moisture contributed only negligible amounts of water to the catchment during the dry season and is not covered by our sampling. Therefore, it is not further evaluated here. Pre-ISM 1-week (168 hr) trajectories are derived from close range, with the bulk of moisture sourced from roughly within a 500 km radius in the Himalayan foreland (Figure 4a). During the ISM, moisture sources for precipitation in Lete were distributed along trajectories of >1,000 km length, originating from the Arabian Sea and Bay of Bengal, with additional input from the Himalayan foreland (Figure 4b). Ratios of the straight-line trajectory length (distance between start and end point) and the track length show that ISM trajectories are relatively linear with mean ratios of 1.65. Pre-ISM, with a mean ratio of 3.19, has much more winding trajectory paths (Tables S7 and S8 in Supporting Information S1). Subsequent alterations to pre-ISM water isotope ratios via continental moisture recycling are discussed in Section 4.1.

3.3. Observed Catchment River Discharge

Discharge increases from Lete to Purtighat by an order of magnitude. Both hydrographs are characterized by a typical monsoon pattern with low discharge during winter and high discharge during ISM. Average low flow at Lete was ~16 m^3/s and increased on average to ~81 m^3/s during ISM (Figure 2). At Purtighat, downstream of the orographic barrier, the equivalent average values were ~68 to ~688 m^3/s. As mentioned above, 2015 is anomalous compared to other years, with ISM discharge below 1 σ of the mean with ~80 m^3/s at Lete and ~162 m^3/s at Purtighat. At Purtighat, 2015 winter (~80 m^3/s) and pre-ISM (~99 m^3/s) discharges were 1-σ above the mean (Tables S9 and S10 in Supporting Information S1). Note that winter and pre-ISM interannual discharge comparisons are not possible for Lete because of extended periods with no data.

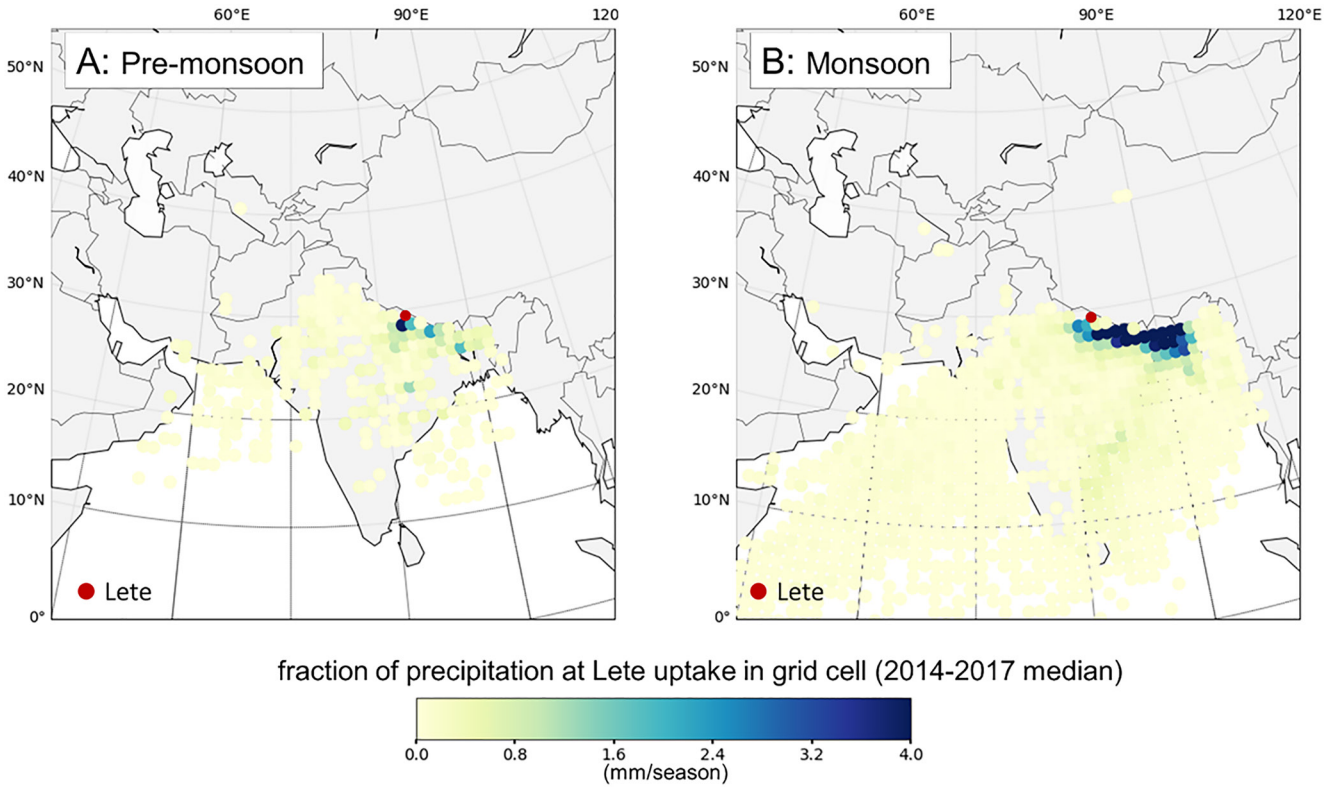

Figure 4. Fractional moisture uptake contribution to rain at Lete gridded at a 1° resolution (Text S1 in Supporting Information S1) derived from Hysplit trajectories (Figure S9 in Supporting Information S1). Pre-monsoon (a) has moisture sources more local than monsoon (b) during the four investigated years. Seasonal variability in moisture uptake exists for both the monsoon (b) and pre-monsoon (a) throughout the time series duration (Figure S10 in Supporting Information S1). Measurements of the trajectories themselves show that Indian Summer Monsoon (ISM) trajectories are relatively linear with ratios of the track length to the straight-line trajectory length (distance between start and end point) of 1.65. Pre-ISM, with a mean ratio of 3.19, has much more winding trajectory paths (Tables S7 and S8 in Supporting Information S1).

3.4. End-Members Contributing to River Discharge

At Lete, located at the orographic barrier, rain δ^2H median values ranged from +21.0‰ in May, −97.7‰ in July, and −81.6‰ in October on average in our 2-year data set (Figure S1 and Table S11 in Supporting Information S1). All data plot along the GMWL (Figure 3) therefore we report only δ^2H in the main text. D-excess medians fall in the range of 18.9‰ in May, 11.2‰ in July, and 15.0‰ in October (Figure S2 and Table S11 in Supporting Information S1).

The isotopic composition of rainwater sampled in Kathmandu, in front of the orographic barrier, showed a similar seasonal trend, but with lower δ^2H and d-excess median values. In April, δ^2H was 8.7‰ and d-excess 13.0‰ (Figures S1 and S2, Table S12 in Supporting Information S1). Lowest values were recorded in August, with δ^2H −74.5‰ and d-excess 8.7‰.

Snow samples had a median δ^2H of −100.7‰ along a spatial trend with a decrease from δ^2H −72.4‰ at the orographic barrier to −120.7‰ northward (Tables S13–S15 in Supporting Information S1). Across the same gradient, d-excess decreased from 16.9‰ to 13.7‰, with a median catchment value of 14.7‰. Glacier samples had a median δ^2H and d-excess of −129.7‰ and 15.2‰, respectively.

Finally, groundwater-fed springs had a median δ^2H of −68.6‰, and d-excess of 10.9‰ (Tables S13–S15 in Supporting Information S1). Spring δ^2H values decreased from −58.1‰ south of the orographic barrier to −80.8‰ farther north, while d-excess increased from 9.4‰ to 12.2‰. Hotsprings had a median δ^2H of −73.7‰ and d-excess of 10.6‰, typically in the same range as groundwater springs.

To compare water source end-members (rain, springs, snow, and glacier), Figure 5b shows the data plotted in a d-excess versus δ^2H framework, with the mean and convex hull for each end-member. Monthly averages for rain were calculated for data from Lete (gray) and Kathmandu (blue) for 2016 and 2017 (Figure 5a). The

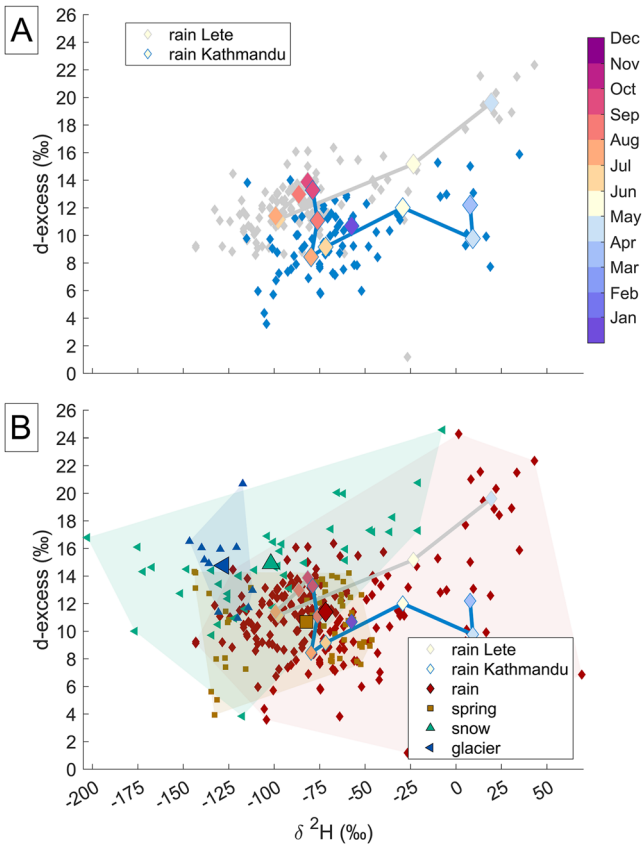

Figure 5. Seasonal water end-members in d-excess versus δ^2H space. (a) Seasonal variation of rain samples in Lete (gray diamonds) and Kathmandu (blue diamonds). Colored diamonds outlined in gray (Lete) and blue (Kathmandu) represent mean monthly values. There is a systematic increase in d-excess from Kathmandu to Lete. (b) Water sources including rain (red diamonds), groundwater spring including hotsprings (brown squares), snow (green triangle), and glacier (blue triangles) stable isotope samples are plotted. Larger symbols with black outlines are means of each water source and are enclosed in convex hulls, marking the range of each water source. Pre-monsoon rain samples occupy a unique sample space with both high d-excess and δ^2H (light blue to yellow diamonds). While springs are similar in space to monsoon rain samples, both snow and glacier samples have higher d-excess values and are generally more negative in δ^2H (Figure S3 in Supporting Information S1).

seasonal variability of rain water composition indicates an overall decrease in d-excess and δ^2H values from May to August and an increase in d-excess from September to October. Lete rain samples were offset to more positive values in d-excess from Kathmandu samples for all months except October (Figure 5a). On average, Lete δ^2H rain values were ~19‰ more negative than those from Kathmandu in July, August, and September. Similar in space and time to rain samples, groundwater-fed spring samples were more negative in δ^2H and had higher d-excess values behind the orographic barrier. Compared to snow and glaciers, ISM rain and spring samples tended to have lower d-excess and less negative δ^2H (Figure S3 in Supporting Information S1).

3.5. Spatial Variability in River Discharge

We observe a latitudinal trend with progressively decreasing δ^2H river isotope values from south to north across the Himalayan range (latitudinal lapse rate: −55.3‰/°, Figure 6a). At similar elevation or latitude, river samples were characterized by more negative δ^2H values compared to local tributaries, springs, and rain (Figure 6a). Even tributaries draining the very high elevations (>6,000 masl.) had more positive δ^2H values than the main river at the same latitude. Across the headwaters, northernmost part of the study area, where the mean elevation is constant, δ^2H river values followed a lower latitudinal lapse rate of −7.3‰/°. This offset between the river and its tributaries reflects the integration of more negative isotopic values from upstream; meanwhile, tributaries reflect the local precipitation isotopic signature (Garzione et al., 2000). At the headwaters, tributaries, rain, and springs share the most negative δ^2H values. As the Kali Gandaki river flows from north to south, it integrates these upstream inputs with more positive δ^2H local precipitation and tributary contributions, causing the river δ^2H values to increase progressively downstream (Figure 6a).

D-excess varied non-linearly across the orographic barrier. Overall, highest d-excess (13.8‰) values in river samples were observed just south of the highest elevation band (28.6°) and decreased both to the north and south (Figure 6b, black solid line, $p < 0.00001$; Text S4 in Supporting Information S1). Seasonal measurements show that the latitudinal pattern of d-excess values was maintained throughout most of the year.

3.6. Seasonal Variability in River Discharge

The river water isotope data is characterized by strong seasonal variability, where late-ISM and winter have the lowest δ^2H values (Figure 2). Catchment d-excess ranges (6.1‰–18.0‰) are comparable to seasonal ranges at both Lete (8.6‰–22.4‰) and Purtighat (10.9‰–18.0‰) (Figure 2). Pre-ISM samples have enriched δ^2H values along the latitudinal gradient (Figure 6). In most years, the lowest d-excess and δ^2H river water isotope values occurred in the mid ISM (Figure 2). Throughout the pre-ISM, d-excess and δ^2H values increase, and then subsequently decrease at the start of ISM. This trend can be represented with a counterclockwise hysteresis loop (Figure 7). In 2015, both Purtighat and Lete did not have a large hysteresis loop, highlighting a fundamental change in the hydrological drivers in the catchment during this year. Additional to this large hysteresis loop, we occasionally observed an additional negative δ^2H excursion of ~15‰ from June to August with constant d-excess values (Figure 7). This negative excursion was observed at Lete and Purtighat in 2016, at Lete 2014 and 2017, and was not found in 2015 (Figure 7). The lack of an excursion for Purtighat in 2014 and 2017 might be partially due to sparse data (Figure 2).

3.7. Modeling Seasonal and Latitudinal Precipitation Variability in the Catchment

The single-column rainout model shows a decreasing δ^2H and an increasing d-excess with increasing latitude for all seasons (Figure 8, Figure S4 in Supporting Information S1). North of the orographic barrier, 28.7°N,

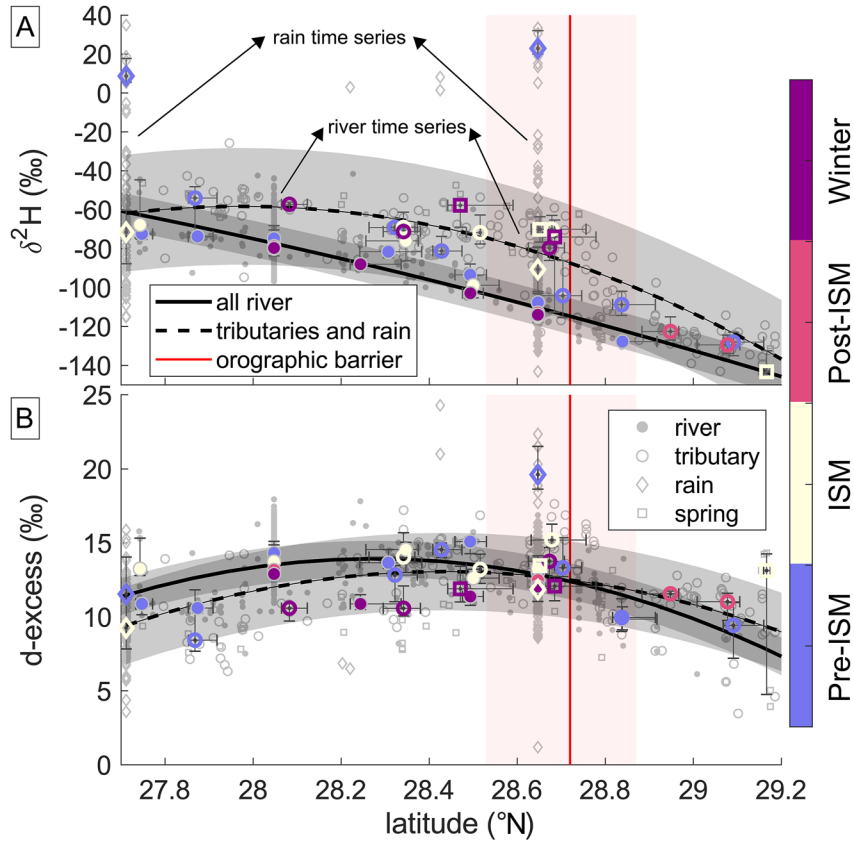

Figure 6. Latitudinal gradient in water stable isotope (a) δ^2H and (b) d-excess. Gray samples are all available data with symbols referring to water types. Median isotopic and latitude values are plotted in bigger symbols for 0.2° bins and each season, but only if five samples are found within those constraints. Error bars for bigger symbols refer to 25% and 75% percentiles. Second degree polynomial fits of all river (solid black lines) and spring and rain (dashed black lines) samples are given for both plots, except for river δ^2H versus latitude, which has a linear fit (see Text S4 in Supporting Information S1). Shading indicates 1-σ uncertainty of fit. Seasonal variability is best seen in time series data at Kathmandu (27.71°N), Purtighat (28.05°N), and Lete (28.65°N). The red vertical line indicates the orographic barrier at 28.7°N with bounds of 28.5° and 28.9°N latitude. Panel (a) shows the decrease in δ^2H with increasing latitude as moisture becomes isotopically lighter. Spring and tributary samples plot above river sample values, hinting at mixing of upstream (more negative) water with tributary values (more positive). Rivers can have up to 50‰ in δ^2H and 7‰ in d-excess seasonal variation at one location. Panel (b) shows an increase in end-member (spring/tributary/rain) samples (dashed-line) d-excess until 28.5°N for most of the year (except May–June) and a decrease in d-excess after 28.5°N. The maximum in the concave up d-excess versus latitude shape is shifted to the left for river values compared to tributary and spring samples.

the δ^2H values level to a constant value. Here, this pattern follows the average elevation trend that also stays relatively constant (Figure 6a). The pre-monsoon model run has the highest d-excess values overall (light blue line, Figure 8). Enabling a rain re-evaporation component in the model similar to Li and Garzione (2017) does not significantly change the δ^2H model runs for all seasons (Figure S4 in Supporting Information S1). D-excess decreases systematically in the rain re-evaporation enabled model compared to the model without rain re-evaporation for all seasons, consistent with theory (Stewart, 1975).

4. Discussion

We first discuss moisture delivery to the Kali Gandaki catchment, and how seasonality in moisture sources affects the isotopic signature of local precipitation. Subsequently, we evaluate how the signature of precipitation compares to different water storage reservoirs. We show that rivers carry the ISM precipitation signature throughout the year except for during the Pre-ISM, pointing toward a dominant, well-mixed groundwater reservoir. With this information, we interpret the seasonal river isotope cycle at our two 4-year continuous measuring stations, highlighting the distinct isotopic signature of the pre-ISM precipitation. This finding is contrasted by the rather stable ISM isotopic signature. Next, we discuss the interannual variability of the system in the context

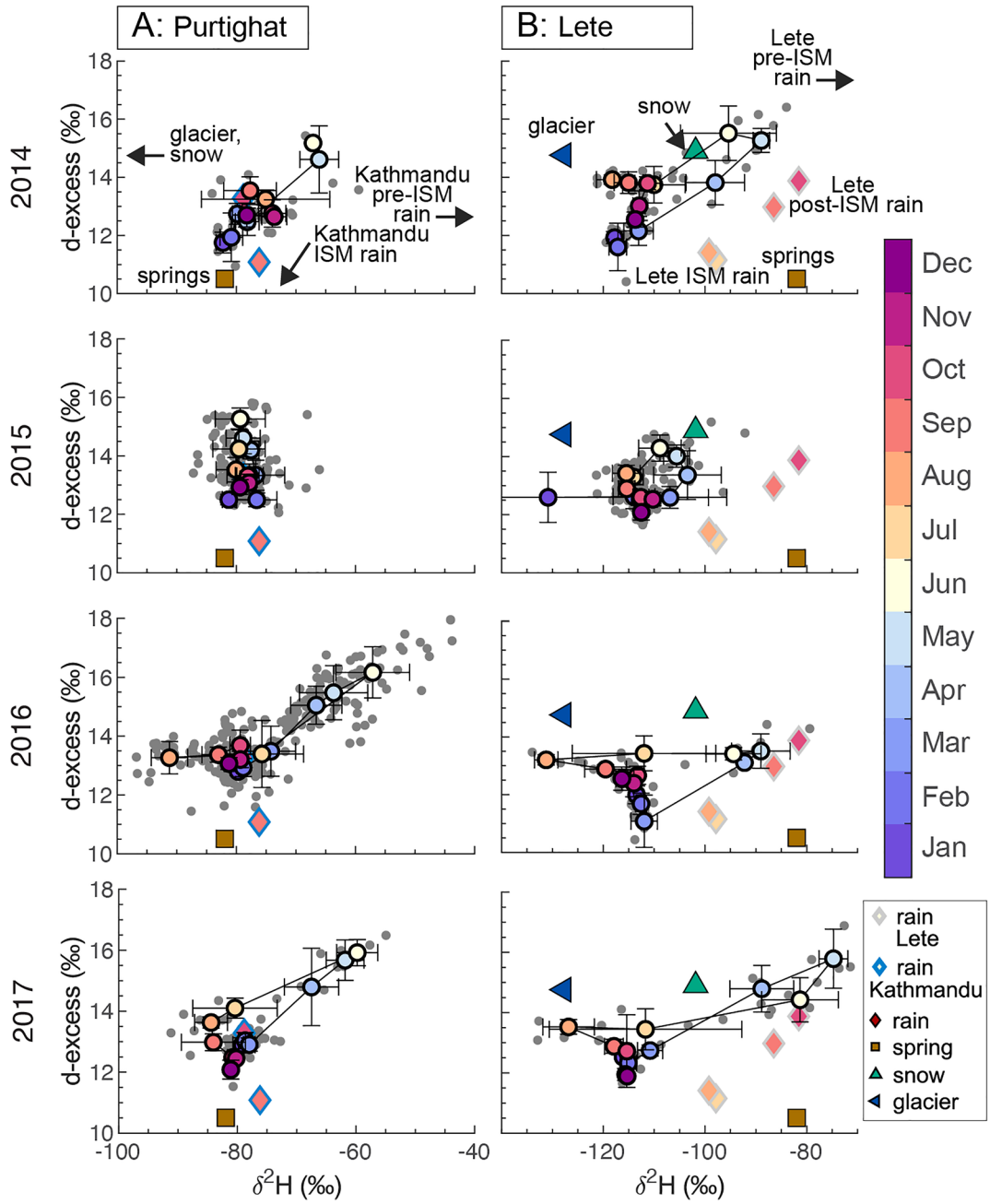

Figure 7. Seasonal and interannual stable isotope variability for Purtighat (column a) and Lete (column b) river samples with end-member (rain, groundwater springs, snow, and glacier) means (see Figure 5 for details). Note the different scaling on the *x*-axis. For Lete and Purtighat in 2014 and 2016, a positive δ^2H and d-excess for April–June shows that most of the seasonal variability in river isotopes originates from the pre-monsoon (April–mid June) period. In 2015, the large positive δ^2H trend in the pre-monsoon is dampened for both Lete and Purtighat. Larger colored circles with black outlines and error bars indicate monthly river mean and one standard deviation. Smaller light gray dots indicate all samples for the sample location and year.

of contrasting hydroclimate between the four observation years. Finally, we discuss the major implications of the prominent pre-ISM signal for the interpretation of stable water isotope-based climate archives in this region.

4.1. Moisture Delivery to the Catchment

We explored the delivery paths of pre-ISM and ISM water vapor to our catchment. The 7-day long HYSPLIT trajectories (Figure 4, Text S1 in Supporting Information S1) show highly seasonal patterns of source pathways,

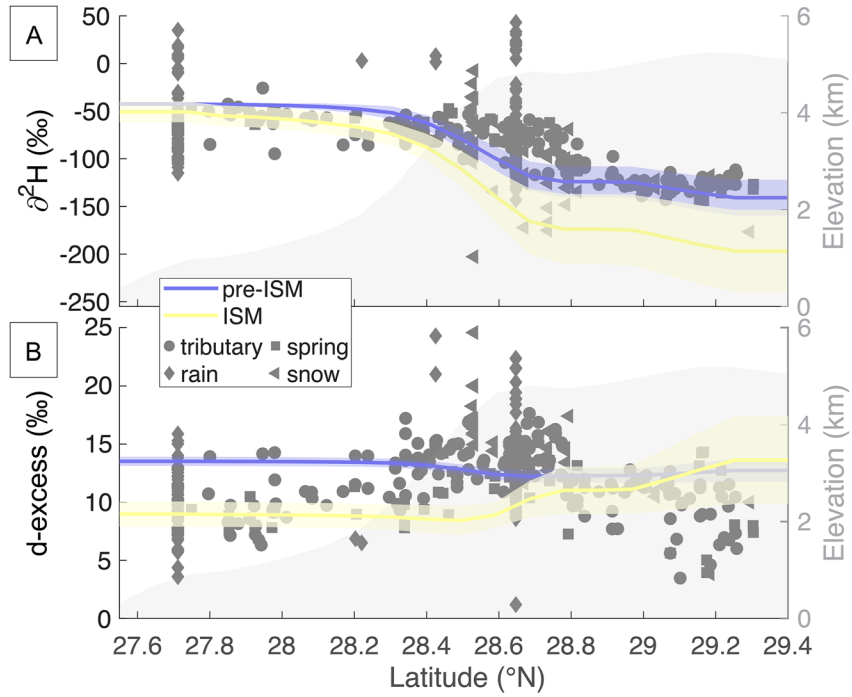

Figure 8. Single column Rayleigh rainout model of (a) δ^2H and (b) d-excess for the Kali Gandaki catchment, using representative isotopic signatures from two different moisture sources: Gangetic Plain (pre-Indian Summer Monsoon [ISM]) and Bay of Bengal (ISM). The lines are model means with shaded 1-σ bounds. The swatch elevation from the High Asia Refined (HAR) analysis data set is plotted in the background, which is one HAR variable used to constrain the model.

characterized by local sources from the Gangetic plain, close to the site of precipitation in pre-ISM, and a mixture of far-afield sources from the open ocean and Gangetic plain during the ISM (Figure 4). These changes in moisture source area and transport distance are reflected in distinct isotopic signatures during the different seasons (Tables S7 and S8 in Supporting Inforation S1, Figure 6a; Brunello et al., 2019; Z. Cai & Tian, 2020).

Winter and post-ISM provide negligible moisture and thus have very little impact on isotopic signals in the region. This is further supported by the isotopic river water signatures during winter, which do not deviate from the typical ISM values (Figure 2). Thus, we do not elaborate further on these two seasons.

The ISM contributes >80% of the annual precipitation via delivery of moisture-laden air from both the Arabian Sea and Bay of Bengal (Tables S1 and S2 in Supporting Information S1, Figure 4). Our results are also indicative of moisture recycling in the Gangetic Plain region during the ISM. The continued moisture uptake in HYSPLIT from the Arabian Sea and Bay of Bengal to the study area is likely due to fast moisture propagation, traveling from the source region to the destination for the season. Rainfall during ISM has very light δ^2H signatures and low d-excess values, also reflected in the river water, and is the product of a relative direct delivery pathway that can extend 1,000s of kilometers away from the catchment.

In contrast, during pre-ISM (~10% of annual precipitation), vapor delivered to the catchment is recycled via evaporation and convective precipitation originating mainly from the Gangetic Plain (Tuinenburg et al., 2012; Z. Cai et al., 2018). Our HYSPLIT modeling shows that the 168 hr trajectories are stationary over the Gangetic plain, thus likely incorporating several recycling periods. This stationary cycling imparts a unique water stable isotope signal on precipitation by enriching ^{2}H and ^{18}O in the moisture source region via kinetic fractionation during evaporation, which leads to more positive δ^{18}O, δ^2H, and d-excess values in the landscape. Surface waters in the Gangetic plain during pre-ISM have a strongly enriched isotopic composition (Gajurel et al., 2006; Kumar et al., 2019; Mukherjee et al., 2007; Figure 3). Hence, moisture sourced from these reservoirs has more positive δ^2H values and higher d-excess values. Z. Cai et al. (2018) showed that convection amount drives a more positive δ^{18}O signature in precipitation in source regions such as the Bay of Bengal and the northern South China Sea. However, to-date, the importance of continental moisture recycling for different seasons in the central Himalayas

has not been evaluated, and continuous sampling observations with seasonal and/or sub-seasonal resolution are sorely lacking.

Usually, high d-excess values in precipitation over the region are attributed to Mediterranean moisture (i.e., Karim & Veizer, 2002), transported by the disturbance-derived Westerly. In contrast, our data suggests that pre-ISM moisture that has been recycled via evaporation on the Gangetic plain may provide an alternative explanation for elevated d-excess.

4.2. Precipitation Isotope Signatures Within the Catchment

The precipitation rainout pathway in the Kali Gandaki catchment ramps up against the Himalayan topographic gradient (Figure 1). The isotopic gradient in rainfall is inverse of the topography, with progressively more negative δ^2H and $\delta^{18}O$ values toward the north (Figure 6a). These values follow rainout trends observed when moisture is forced to condense via adiabatic uplift across orographic barriers and can be described in the Rayleigh distillation framework. Behind the orographic barrier, topography remains within a limited elevation range, reflected in a flattening of the trend in isotopic δ^2H of rain and tributary discharge in the headwaters (Figure 6a). Our Rayleigh distillation model replicates δ^2H decreases across the orographic barrier and shows a decrease in isotopic change as topography gradients decrease in the north (Figure 8). As such δ^2H is a function of the altitudinal profile across the catchment and is determined by adiabatic uplift and rainout of moisture.

Interpreting the increase in rainfall d-excess from the south toward the orographic barrier (Figure 6b) is more difficult. Currently, the observed concave downtrend in d-excess versus latitude cannot be explained by our Rayleigh distillation model (Figure 8b). Thus, this discrepancy points toward other fractionation processes that need to be explored. Plausible explanations include winter/pre-ISM snow, rain re-evaporation, and lower temperature condensation (Bershaw et al., 2012). The high d-excess values we refer to Rayleigh distillation processes at low cloud temperatures when non-equilibrium processes such as diffusion of water vapor on ice droplets might be significant (Ciais & Jouzel, 1994; Lacelle, 2011). We deem this the most plausible explanation of our observations, which is well in line with the latest findings by Bershaw (2018). Lete is located at a higher elevation and latitude than Kathmandu and also generally has higher rain d-excess monthly means (Figure 5a). Our single-column model shows a latitudinal increase in precipitation d-excess toward the orographic barrier for ISM moisture sources for with and without rain re-evaporation (Figure 8b, Figure S4 in Supporting Information S1). However, neither the ISM nor pre-ISM model can reproduce the range of increase in d-excess with increasing latitude. We expect larger increase in d-excess is likely due to both lower cloud temperatures and higher rainout fractions than the modeling suggests (Figures S5 and S6 in Supporting Information S1).

North of the orographic barrier we observe a decrease in d-excess (Figure 6b), which coincides with a region where very little precipitation occurs (Figure 1b). It is likely that rain re-evaporation occurs due to drier atmospheric conditions and counteracts the increasing trend in d-excess observed south of the orographic barrier. However, our modeling efforts to include rain re-evaporation in our single column Rayleigh distillation model have not captured the same magnitude of d-excess decrease (Figure S4 in Supporting Information S1). This observation underlines that complex cloud interactions are hard to reproduce in a simple 1D model. We thus hypothesize that behind the orographic barrier, Rayleigh distillation does not explain the bulk of rain isotopic change, as other processes such as rain re-evaporation likely contribute to modification of moisture. These changes occur in a zone with smaller elevation gradients, where moisture is not forced to uplift adiabatically, as it is in the front of the orographic barrier, where Rayleigh distillation dominates. Given the systematic changes in d-excess across the catchment (Figure 6b), catchment-scale moisture transport and condensation processes likely overprint moisture source d-excess signatures.

4.3. Catchment-Scale Water Isotopes Point Toward a Well-Mixed Groundwater Reservoir

There is a stark contrast between the variability of δ^2H river isotopes (40‰–60‰) at both sampling locations and rainfall isotopic variability that is almost three times larger, ranging in δ^2H from >21.0‰ to almost −100‰ (difference of ∼120‰). This contrast in river isotopic range suggests a large and well mixed intermediate reservoir, buffering rainfall and river. River baseflow during the dry season (post-ISM to pre-ISM) has stable isotope values (Figure 2c) similar to groundwater-fed springs (Figures 4 and 5a, Figure S3 in Supporting Information S1). Given the similar isotopic composition between the range of ISM rain and groundwater, groundwater is likely

recharged predominantly during the ISM (Figures 2, 5a and 7). The stored groundwater is progressively released by gravity-driven drainage through the dry season. Hence, we propose that groundwater recharge is the most important buffer mechanism in the Himalayan water cycle. This supports findings by Jasechko et al. (2016) that mountains release older water and river discharge in the Himalayas is up to ∼2/3 groundwater-fed (Andermann, Longuevergne, et al., 2012).

The $\delta^{18}O$ versus $\delta^{2}H$ plot (Figure 3) shows that measurements from all hydrological compartments within the catchment, regardless of seasonality, plot along a common meteoric water line similar to the Global Meteoric Water Line (Sharp, 2017). We do not observe any systematic deviation pointing to overprint by widespread evaporation or other processes influencing the isotopic composition of surface water (Figure S7 in Supporting Information S1). If waters undergo evaporative processes from precipitation to river discharge, the relative evaporative fraction will produce an offset from the global and/or local meteoric water line toward higher $\delta^{18}O$. This would be expressed as an offset, as observed in the Gangetic plain surface waters (e.g., Figure 3; Benettin et al., 2018). Evaporation from soils does not appear in discharge forming pathways. Illien et al. (2021) show that throughout the seasonal cycle in Nepal, the shallow groundwater zone acts as a buffer; as cumulative rainfall increases to a specific threshold, rainfall is transferred to groundwater, eliminating atmospheric interaction. While we cannot rule out evaporation processes in the landscape (e.g., north of the orographic barrier), our observation suggests that evaporatively enriched waters are not connected with the active hydrological cycle and are negligible for river water.

Himalayan water resources are often viewed through the prism of glaciers and glacier mass loss due to climate change (Brun et al., 2017; Immerzeel et al., 2010, 2013; Lutz et al., 2014). However, our findings contest the importance of glaciers for the perennial water availability for the downstream regions of the Nepal Himalayas. Boral and Sen (2020) suggest, for example, based on stable isotope measurements, a dominance of glacier melt contributions to dry season river discharge. Several other studies have reached similar conclusions using similar observations, and neglect groundwater as an important reservoir (Bookhagen & Burbank, 2010; Immerzeel et al., 2010; Wulf et al., 2016). In the Kali Gandaki catchment, glacial coverage is ∼10% or less of the total area, but precipitation is widespread and intense, making a large contribution from glacial melt unlikely for the central Himalayas. In particular, during the dry season, when water resources are most needed and discharge is very low, water appears to be sourced from a rather stable and well mixed reservoir that we interpret as groundwater. At the same time, the dry season coincides with winter, where most of the glaciers are frozen and melting is limited by low temperatures. However, this season is most pertinent as river discharge is low and rainfall is limited. Our findings demonstrate that the subsurface component in the Himalayan water cycle requires further constraints to adequately prepare for future climate change, a conclusion which likely holds for the wider Himalayan region and other mountain belts.

4.4. Pre-ISM Moisture Supply Governs Seasonality of Water Stable Isotopes

The water stable isotope seasonality of rain and river waters is largely driven by pre-ISM moisture supply. Pre-ISM is the most isotopically distinct season as reflected in rain and river discharge (Figures 2 and 5a) across the entire orographic barrier. Pre-ISM rainfall during May and the beginning of June is characterized by positive isotopic signatures (19.4‰ $\delta^{2}H$ and d-excess 19.6‰), which rapidly decrease to distinct negative ISM signatures (−97.9‰ $\delta^{2}H$ and d-excess 11.2‰) after the onset of the summer ISM (Figure 2). This strong contrast between pre-ISM and the rest of the year dominates all other signatures in the catchment and is even stronger than the spatial pattern across the Himalayan range, the largest orographic barrier on Earth (Figure 6). Locally sourced pre-ISM moisture that has been recycled on the Gangetic plain provides context for high d-excess and positive $\delta^{2}H$ observations (see Section 4.1).

There is a distinct winter to pre-ISM to ISM mixing line in the river d-excess versus $\delta^{2}H$ framework for the Kali Gandaki catchment (Figure 7). During the dry season, the river isotopic composition aligns with relatively lower $\delta^{2}H$ and d-excess values of groundwater, which is at this time the main source of water (Figure 7). As precipitation begins to increase during pre-ISM and when baseflow river discharge is still relatively low (Figure 2), the distinct high $\delta^{2}H$ and d-excess isotopic values of the pre-ISM precipitation (Figure 5) propagate into the river water isotopic values (Figure 7). This observation suggests that some precipitation runs off directly, which is supported by Illien et al. (2021), who have found that in the pre-ISM period the groundwater reservoir is not recharged by precipitation. Instead, these authors show that groundwater recharge starts in ISM. The maximum

and minimum of river isotope values are defined by pre-ISM continentally recycled precipitation and groundwater recharged by ISM rainfall as well as more upstream precipitation. This mixing line highlights the importance of precipitation during the pre-ISM and ISM seasons as river discharge sources (Figure 5a).

A smaller magnitude trend in the river d-excess versus δ^2H framework occurs during some ISM. The river δ^2H values decrease by ~15‰ from June to July and increase in August while d-excess remains constant (Figures 5a and 7). Glaciers have low δ^2H signatures and typically melt during the summer months. Thus, glacier melt could explain the negative excursion of δ^2H. This interpretation would be consistent with the melt period of glaciers in the Himalayas (Boral & Sen, 2020; Wulf et al., 2016). However, this isotope signature is also recorded in nearby non-glaciated catchments (Illien et al., 2021), suggesting other drivers to be important. We find no correlation between GPM rain precipitation and δ^2H rain values (Figure S8 in Supporting Information S1). We interpret this occasionally occurring signature as a result of greater rain contribution to river discharge from high elevation rain. δ^2H and d-excess values are elevation-dependent and more negative and more positive, respectively, at higher elevations. The orographically induced precipitation peak in Nepal is located at around 4 km elevation (Andermann et al., 2011; Bookhagen & Burbank, 2006) supporting our findings. However, it is difficult to explain the negative δ^2H isotope excursion with no change in d-excess with a single process. A combination of several mechanisms is the most likely explanation.

The strong seasonality caused by pre-ISM moisture delivery across the entire mountain range raises questions about the interpretation of water isotopes in paleoclimatic proxy systems. Stable water isotopes, preserved in mollusks, lake sediments, tree rings, paleo soils, stalagmites, and ice cores, have been established as one of the key recorders of past ISM strength (Botsyun et al., 2019; Gajurel et al., 2006; Licht et al., 2014; Menges et al., 2019; Taft et al., 2012; Y. Cai et al., 2015). More recently this notion of exclusive ISM preservation through stable water isotope records has been challenged by studies pointing out seasonal variability and the potential shared impact on the preserved isotopic signatures (Breitenbach et al., 2010; Brunello et al., 2019; Wolf et al., 2020; Z. Cai et al., 2017). Brunello et al. (2019) showed how $\delta^{18}O$ is preserved in tree rings at the orographic barrier in Lete record pre-ISM and ISM rainfall. Similarly, Breitenbach et al. (2010) showed that the isotopic signature at the Shillong Plateau depends strongly on the amalgamation of ISM and pre-ISM. To apply our findings of a strong seasonality in water isotopes, future work will require a process-based understanding of how water isotope signals are propagated into individual paleoclimate archives.

Our detailed time series, encompassing four contrasting ISM seasons, confirms and quantifies the influence of different seasons on the annual isotopic budget. For example, in 2015 ISM rainfall is weak and there is almost no pre-ISM rainfall. The low isotopic water values would be recorded as a "strong" ISM year in most paleoclimatic interpretations. In contrast, 2017 had a similarly weak ISM but a well-defined pre-ISM isotopic signature (Figure 2), which would lead to a starkly different preservation signature. These findings provide useful insights for the interpretation of high temporal resolution climate archives with respect to seasonality.

4.5. Potential Impacts of ENSO and Snow Melting on River Water Isotopic Excursion

Seasonal precipitation variability in the Himalayan region is linked to modes of global climate variability. Modeling studies show that moisture availability in the Himalayan foreland, including the Gangetic Plain, influences the local climate and the atmospheric humidity, in particular during pre-ISM (Ambika & Mishra, 2020; Mishra et al., 2020). In the Gangetic Plain, the source of pre-ISM precipitation for our study site, droughts tend to occur during El Niño years, including in 2015 (Mishra et al., 2020). For Nepal, Pokharel et al. (2020) showed that 35% of all precipitation variability can be associated with El Niño-Southern Oscillation (ENSO) such that there is more precipitation during La Niña years. Pre-ISM and ISM precipitation patterns across sub-catchment were more consistent with these predictions for El Niño (2014–2016) than those during La Niña (2016, 2017) years (Tables S1, S2, S9 and S10 in Supporting Information S1), with the drought showing up in ISM precipitation and the discharge at Purtigaht in 2015 (Table S9 in Supporting Information S1). The sampling years presented here include both El Niño and La Niña years with no isotopic record taken during neutral years. Further sampling efforts can help unravel the teleconnections to ENSO in the study area and assess isotopic and precipitation variability beyond ENSO years.

During the 2-year 2014-2015 El Niño event, snowfall was at a record high throughout post-ISM 2014 to pre-ISM 2015 (Figure 2, Tables S9 and S10 in Supporting Information S1), a 100-year event (Fujita et al., 2017). We

cannot link this snowfall to El Niño, but the record needs to be considered in this context. Most snow samples are isotopically distinct from rain samples, with higher d-excess and lower δ^2H values (Figure 5b). Elevated snowfall during winter and pre-ISM 2015 resulted in higher river discharge during this period (Figure 2, Tables S9 and S10 in Supporting Information S1). The ~5‰ difference in river δ^2H values during pre-ISM 2015 compared to other years was likely derived from increased snowmelt, which has more negative δ^2H values than pre-ISM rain. Discharge also increased in winter 2014 and pre-ISM 2015 in Purtighat (Table S3 in Supporting Information S1) alongside more negative river pre-ISM δ^2H values, consistent with increased snowmelt. Thus, the year 2015 likely represents an upper bound on snow melt contribution to the hydrological system in the central Himalayas.

5. Conclusions

In this work, we present a comprehensive spatiotemporal stable water isotope data set, spanning all water sources across the central Himalayan orographic barrier. We document seasonality in river flow and moisture pathways to the catchment during four consecutive, meteorologically contrasting sampling years. During the dry season, the consistent stable isotope signature of the river water points toward a well-mixed groundwater reservoir. The lack of substantial deviations from the meteoric water line of all water samples suggests that evaporative processes on the landscape do not propagate into river hydrological cycle. We additionally find that, at the end of the dry season, pre-ISM precipitation is the most contrasting water stable isotope signature, characterized by positive isotope values. The pre-ISM originates from Gangetic Plain moisture that likely undergoes several evaporation-precipitation cycles of moisture recycling. Furthermore, the large variability in ISM precipitation amount throughout the 4 years did not result in a distinct river water stable isotope signature over the years.

ISM precipitation and groundwater, combined with pre-ISM precipitation, control the entire water system and regional water availability in this area of the central Himalayas. The ISM contributes the largest precipitation amount annually, and thus saturates the hydrological system with its isotopic signature. ISM rainfall recharges groundwater reservoirs and maintains water availability throughout the rest of the year. Isotope analysis of end-members contributing to river discharge underscores groundwater as a principal reservoir, with minimal contributions from glacier melt, even in a catchment comprising two of the highest, most glaciated peaks of the mountain belt.

Our data set constrains a characteristic range of spatiotemporal and seasonal variability in stable water isotopic signatures in the Himalayan surface system and provides a broad basis for an improved understanding of the regional water cycle. The pre-ISM precipitation signal reaches far north into, and beyond the High Himalayas, even where annual precipitation decreases drastically. Our data suggest that pre-ISM precipitation variability—instead of the ISM strength—is the characteristic signal across the catchment. As previously shown by Brunello et al. (2019), pre-ISM is imprinted in paleoclimate records with high temporal resolution (e.g., tree rings, stalagmites, mollusk shells, and ice cores). Additional monitoring campaigns during pre-ISM are thus critical for refining the interpretation of water isotope-based paleoclimate records. Future paleoclimate record interpretation should consider pre-ISM moisture pathways and associated Gangetic Plain climatology to enhance understanding of global climate change signatures.

Finally, the greater Himalayan region sources water to most major rivers on the Asian continent, a freshwater source critically affected by climate change. By providing regional constraints, using water isotopes, on local hydrological pathways, this study lays the groundwork for refining projections of water supply in mountain hydrological systems such as the Himalayas, with implications for water resource management.

Conflict of Interest

The authors declare no conflicts of interest relevant to this study.

Data Availability Statement

The field data, sampling and analytical procedures are published separately at the GFZ Data Services and available at https://doi.org/10.1029/2011GC003513 under the creative commons 4.0 license (Anderman et al., 2021). The Kali Gandaki High Mountain Observatory, Stable Water Isotope database can be accessed as a zip file under the Files column Download data link. The GPM_3IMERGHH data is available at the NASA/Goddard Space Flight Center's GES DISC (Huffman et al., 2019). High Asia Refined analysis (HAR) data is available through

TU Berlin, Berlin, Germany, from their website at https://www.klima.tu-berlin.de/index.php?show=daten_har (Maussion et al., 2011, 2014). NCEP-NCAR Reanalysis 1 data, used to determining isotopic modeling initial parameters, is available the NOAA PSL, Boulder, Colorado, USA, from their website at https://psl.noaa.gov (Kalnay et al., 1996).

Acknowledgments
The authors thank Bhairab Sitaula, Pratikshya Gautam, Basanta Raj Adhikari, and Johanna Menges for help collecting field data. The authors thank Carolin Zorn (GFZ) and Mikaela Weiner (AWI Potsdam ISOLAB Facility) for analyzing water isotope samples and Iris van der Veen for helpful discussion of the data. Samples at Lete and Mirmi/Purtighat were taken by Dhan Bahadur and his family and by Ram Hari Sharma and the Kali Gandaki hydropower lab team, respectively. The authors thank John Bershaw and three anonymous reviewers for their feedback. This study was funded by the Helmholtz Impulse and Networking Fund. HHG was supported by the Watson Foundation for her travel funding to Nepal and by the NSF GRFP (DGE-1610403) and the Jackson School of Geosciences subsequently. CA benefitted from the Helmholtz Postdoc Program (PD-039) from the German Helmholtz Association. SD was supported by the University of Texas, Institute for Geophysics Postdoctoral Fellowship. Open Access funding enabled and organized by Projekt DEAL.

References

Ambika, A. K., & Mishra, V. (2020). Substantial decline in atmospheric aridity due to irrigation in India. *Environmental Research Letters*, *15*(12), 124060. https://doi.org/10.1088/1748-9326/abc8bc

Andermann, C., Bonnet, S., & Gloaguen, R. (2011). Evaluation of precipitation data sets along the Himalayan front. *Geochemistry, Geophysics, Geosystems*, *12*(7). https://doi.org/10.1029/2011GC003513

Andermann, C., Crave, A., Gloaguen, R., Davy, P., & Bonnet, S. (2012). Connecting source and transport: Suspended sediments in the Nepal Himalayas. *Earth and Planetary Science Letters*, *351–352*, 158–170. https://doi.org/10.1016/j.epsl.2012.06.059

Andermann, C., Hassenruck-Gudipati, H., Menges, J., Brunello, C. F., Meyer, H., Rach, O., et al. (2021). *Kali Gandaki High Mountain Observatory, Stable Water Isotope database*. GFZ Data Services. https://doi.org/10.5880/GFZ.4.6.2021.004

Andermann, C., Longuevergne, L., Bonnet, S., Crave, A., Davy, P., & Gloaguen, R. (2012). Impact of transient groundwater storage on the discharge of Himalayan rivers. *Nature Geoscience*, *5*(2), 127–132. https://doi.org/10.1038/ngeo1356

Benettin, P., Volkmann, T. H. M., Von Freyberg, J., Frentress, J., Penna, D., Dawson, T. E., & Kirchner, J. W. (2018). Effects of climatic seasonality on the isotopic composition of evaporating soil waters. *Hydrology and Earth System Sciences*, *22*(5), 2881–2890. https://doi.org/10.5194/hess-22-2881-2018

Bershaw, J. (2018). Controls on deuterium excess across Asia. *Geosciences*, *8*(7), 257. https://doi.org/10.3390/geosciences8070257

Bershaw, J., Penny, S. M., & Garzione, C. N. (2012). Stable isotopes of modern water across the Himalaya and eastern Tibetan Plateau: Implications for estimates of paleoelevation and paleoclimate. *Journal of Geophysical Research*, *117*(2), 1–18. https://doi.org/10.1029/2011JD016132

Bookhagen, B., & Burbank, D. W. (2006). Topography, relief, and TRMM-derived rainfall variations along the Himalaya. *Geophysical Research Letters*, *33*(8), 1–5. https://doi.org/10.1029/2006GL026037

Bookhagen, B., & Burbank, D. W. (2010). Toward a complete Himalayan hydrological budget: Spatiotemporal distribution of snowmelt and rainfall and their impact on river discharge. *Journal of Geophysical Research*, *115*(3), 1–25. https://doi.org/10.1029/2009JF001426

Boral, S., & Sen, I. S. (2020). Tracing 'Third Pole' ice meltwater contribution to the Himalayan rivers using oxygen and hydrogen isotopes. *Geochemical Perspectives Letters*, 48–53. https://doi.org/10.7185/geochemlet.2013

Boral, S., Sen, I. S., Ghosal, D., Peucker-Ehrenbrink, B., & Hemingway, J. D. (2019). Stable water isotope modeling reveals spatio-temporal variability of glacier meltwater contributions to Ganges River headwaters. *Journal of Hydrology*, *577*(June), 123983. https://doi.org/10.1016/j.jhydrol.2019.123983

Botsyun, S., Sepulchre, P., Donnadieu, Y., Risi, C., Licht, A., & Caves Rugenstein, J. K. (2019). Revised paleoaltimetry data show low Tibetan Plateau elevation during the Eocene. *Science*, *363*(6430), eaaq1436. https://doi.org/10.1126/science.aaq1436

Breitenbach, S. F. M., Adkins, J. F., Meyer, H., Marwan, N., Kumar, K. K., & Haug, G. H. (2010). Strong influence of water vapor source dynamics on stable isotopes in precipitation observed in Southern Meghalaya, NE India. *Earth and Planetary Science Letters*, *292*(1–2), 212–220. https://doi.org/10.1016/j.epsl.2010.01.038

Brun, F., Berthier, E., Wagnon, P., Kääb, A., & Treichler, D. (2017). A spatially resolved estimate of High Mountain Asia glacier mass balances from 2000 to 2016. *Nature Geoscience*, *10*(9), 668–673. https://doi.org/10.1038/ngeo2999

Brunello, C. F., Andermann, C., Helle, G., Comiti, F., Tonon, G., Tiwari, A., & Hovius, N. (2019). Hydroclimatic seasonality recorded by tree ring $\delta^{18}O$ signature across a Himalayan altitudinal transect. *Earth and Planetary Science Letters*, *518*, 148–159. https://doi.org/10.1016/j.epsl.2019.04.030

Brunello, C. F., Andermann, C., Marc, O., Schneider, K. A., Comiti, F., Achleitner, S., & Hovius, N. (2020). Annually resolved monsoon onset and withdrawal dates across the Himalayas derived from local precipitation statistics. *Geophysical Research Letters*, *47*(23), e2020GL088420. https://doi.org/10.1029/2020GL088420

Cai, Y., Fung, I. Y., Edwards, R. L., An, Z., Cheng, H., Lee, J.-E., et al. (2015). Variability of stalagmite-inferred Indian monsoon precipitation over the past 252,000 y. *Proceedings of the National Academy of Sciences*, *112*(10), 2954–2959. https://doi.org/10.1073/pnas.1424035112

Cai, Z., & Tian, L. (2020). What causes the postmonsoon ^{18}O depletion over Bay of Bengal head and beyond? *Geophysical Research Letters*, *47*(4), 1–10. https://doi.org/10.1029/2020GL086985

Cai, Z., Tian, L., & Bowen, G. J. (2017). ENSO variability reflected in precipitation oxygen isotopes across the Asian Summer Monsoon region. *Earth and Planetary Science Letters*, *475*, 25–33. https://doi.org/10.1016/j.epsl.2017.06.035

Cai, Z., Tian, L., & Bowen, G. J. (2018). Spatial-seasonal patterns reveal large-scale atmospheric controls on Asian Monsoon precipitation water isotope ratios. *Earth and Planetary Science Letters*, *503*, 158–169. https://doi.org/10.1016/j.epsl.2018.09.028

Ciais, P., & Jouzel, J. (1994). Deuterium and oxygen 18 in precipitation: Isotopic model, including mixed cloud processes. *Journal of Geophysical Research*, *99*(D8), 16793–16803. https://doi.org/10.1029/94JD00412

Craig, H., & Gordon, L. I. (1965). Deuterium and oxygen 18 variations in the ocean and the marine atmosphere. In E. Tongiorgi (Ed.), *Stable isotopes in oceanographic studies and paleotemperatures* (pp. 9–130). Consiglio Nazionale Delle Ricerche Laboratorio di Geologia Nucleare. Retrieved from http://climate.colorado.edu/research/CG/CraigGordon1965_Noone_small3.pdf

Cross, M. (2015). PySPLIT: A package for the generation, analysis, and visualization of HYSPLIT air parcel trajectories. *Proceedings of the 14th Python in Science Conference* (pp. 133–137). https://doi.org/10.25080/Majora-7b98e3ed-014

Dinerstein, E., Olson, D., Joshi, A., Vynne, C., Burgess, N. D., Wikramanayake, E., et al. (2017). An ecoregion-based approach to protecting half the terrestrial realm. *BioScience*, *67*(6), 534–545. https://doi.org/10.1093/biosci/bix014

Draxler, R. R. (1999). HYSPLIT_4 user's guide. NOAA Technical Memorandum ERL ARL-230. NOAA Air Resources Laboratory. Retrieved from https://arl.noaa.gov/wp_arl/wp-content/uploads/documents/reports/arl-230.pdf

Fujita, K., Inoue, H., Izumi, T., Yamaguchi, S., Sadakane, A., Sunako, S., et al. (2017). Anomalous winter-snow-amplified earthquake-induced disaster of the 2015 Langtang avalanche in Nepal. *Natural Hazards and Earth System Sciences*, *17*(5), 749–764. https://doi.org/10.5194/nhess-17-749-2017

Gajurel, A. P., France-Lanord, C., Huyghe, P., Guilmette, C., & Gurung, D. (2006). C and O isotope compositions of modern fresh-water mollusc shells and river waters from the Himalaya and Ganga plain. *Chemical Geology*, *233*(1–2), 156–183. https://doi.org/10.1016/j.chemgeo.2006.03.002

Galewsky, J., Steen-Larsen, H. C., Field, R. D., Worden, J., Risi, C., & Schneider, M. (2016). Stable isotopes in atmospheric water vapor and applications to the hydrologic cycle. *Reviews of Geophysics*, *54*(4), 809–865. https://doi.org/10.1002/2015RG000512

Garzione, C. N., Quade, J., DeCelles, P. G., & English, N. B. (2000). Predicting paleoelevation of Tibet and the Himalaya from $\delta^{18}O$ vs. altitude gradients in meteoric water across the Nepal Himalaya. *Earth and Planetary Science Letters*, *183*(1–2), 215–229. https://doi.org/10.1016/S0012-821X(00)00252-1

Gat, J. R. (1996). Oxygen and hydrogen isotopes in the hydrological cycle. *Annual Review of Earth and Planetary Sciences*, *24*(1), 225–262. https://doi.org/10.1146/annurev.earth.24.1.225

Gat, J. R., & Carmi, I. (1970). Evolution of the isotopic composition of atmospheric waters in the Mediterranean Sea area. *Journal of Geophysical Research*, *75*(15), 3039–3048. https://doi.org/10.1029/JC075i015p03039

Hren, M. T., Bookhagen, B., Blisniuk, P. M., Booth, A. L., & Chamberlain, C. P. (2009). $\delta^{18}O$ and δD of streamwaters across the Himalaya and Tibetan Plateau: Implications for moisture sources and paleoelevation reconstructions. *Earth and Planetary Science Letters*, *288*(1–2), 20–32. https://doi.org/10.1016/j.epsl.2009.08.041

Huffman, G. J., Stocker, E. F., Bolvin, D. T., Nelkin, E. J., & Jackson, T. (2019). *GPM IMERG final precipitation L3 half hourly 0.1 degree x 0.1 degree V06*. Goddard Earth Sciences Data and Information Services Center (GES DISC). https://doi.org/10.5067/GPM/IMERG/3B-HH-E/06

Illien, L., Andermann, C., Sens-Schonfelder, C., Cook, K. L., Baidya, K. P., Adhikari, L. B., & Hovius, N. (2021). Subsurface moisture regulates Himalayan groundwater storage and discharge. *AGU Advances*, *2*(2), e2021AV000398. https://doi.org/10.1029/2021AV000398

Immerzeel, W. W., Pellicciotti, F., & Bierkens, M. F. P. (2013). Rising river flows throughout the twenty-first century in two Himalayan glacierized watersheds. *Nature Geoscience*, *6*(9), 742–745. https://doi.org/10.1038/ngeo1896

Immerzeel, W. W., van Beek, L. P. H., & Bierkens, M. F. P. (2010). Climate change will affect the Asian water towers. *Science*, *328*(5984), 1382–1385. https://doi.org/10.1126/science.1183188

Jasechko, S., Kirchner, J. W., Welker, J. M., & McDonnell, J. J. (2016). Substantial proportion of global streamflow less than three months old. *Nature Geoscience*, *9*(2), 126–129. https://doi.org/10.1038/ngeo2636

Jouzel, J., & Merlivat, L. (1984). Deuterium and oxygen 18 in precipitation: Modeling of the isotopic effects during snow formation. *Journal of Geophysical Research*, *89*(D7), 11749. https://doi.org/10.1029/JD089iD07p11749

Kalnay, E., Kanamitsu, M., Kistler, R., Collins, W., Deaven, D., Gandin, L., et al. (1996). The NCEP/NCAR 40-year reanalysis project. *Bulletin of the American Meteorological Society*, *77*(3), 437–471. https://doi.org/10.1175/1520-0477(1996)077<0437:TNYRP>2.0.CO;2

Karim, A., & Veizer, J. (2002). Water balance of the Indus River Basin and moisture source in the Karakoram and Western Himalayas: Implications from hydrogen and oxygen isotopes in river water. *Journal of Geophysical Research*, *107*(18), 1–12. https://doi.org/10.1029/2000JD000253

Kumar, M., Ramanathan, A., Mukherjee, A., Sawlani, R., & Ranjan, S. (2019). Delineating sources of groundwater recharge and carbon in Holocene aquifers of the central Gangetic basin using stable isotopic signatures. *Isotopes in Environmental and Health Studies*, *55*(3), 254–271. https://doi.org/10.1080/10256016.2019.1600515

Lacelle, D. (2011). On the $\delta^{18}O$, δD and D-excess relations in meteoric precipitation and during equilibrium freezing: Theoretical approach and field examples. *Permafrost and Periglacial Processes*, *22*(1), 13–25. https://doi.org/10.1002/ppp.712

Li, L., & Garzione, C. N. (2017). Spatial distribution and controlling factors of stable isotopes in meteoric waters on the Tibetan Plateau: Implications for paleoelevation reconstruction. *Earth and Planetary Science Letters*, *460*, 302–314. https://doi.org/10.1016/j.epsl.2016.11.046

Licht, A., van Cappelle, M., Abels, H. A., Ladant, J.-B., Trabucho-Alexandre, J., France-Lanord, C., et al. (2014). Asian monsoons in a late Eocene greenhouse world. *Nature*, *513*(7519), 501–506. https://doi.org/10.1038/nature13704

Lutz, A. F., Immerzeel, W. W., Shrestha, A. B., & Bierkens, M. F. P. (2014). Consistent increase in High Asia's runoff due to increasing glacier melt and precipitation. *Nature Climate Change*, *4*(7), 587–592. https://doi.org/10.1038/nclimate2237

Majoube, M. (1971). Fractionnement en 180 entre la glace et la vapeur d'eau. *Journal de Chimie Physique*, *68*, 625–636. https://doi.org/10.1051/jcp/1971680625

Maussion, F., Scherer, D., Finkelnburg, R., Richters, J., Yang, W., & Yao, T. (2011). WRF simulation of a precipitation event over the Tibetan Plateau, China – An assessment using remote sensing and ground observations. *Hydrology and Earth System Sciences*, *15*(6), 1795–1817. https://doi.org/10.5194/hess-15-1795-2011

Maussion, F., Scherer, D., Mölg, T., Collier, E., Curio, J., & Finkelnburg, R. (2014). Precipitation seasonality and variability over the Tibetan Plateau as resolved by the high Asia reanalysis. *Journal of Climate*, *27*(5), 1910–1927. https://doi.org/10.1175/JCLI-D-13-00282.1

Meese, B., Bookhagen, B., Olen, S. M., Barthold, F., & Sachse, D. (2018). The effect of Indian Summer Monsoon rainfall on surface water δD values in the central Himalaya. *Hydrological Processes*, *32*(24), 3662–3674. https://doi.org/10.1002/hyp.13281

Menges, J., Hovius, N., Andermann, C., Dietze, M., Swoboda, C., Cook, K. L., et al. (2019). Late Holocene landscape collapse of a trans-Himalayan dryland: Human impact and aridification. *Geophysical Research Letters*, *46*(23), 13814–13824. https://doi.org/10.1029/2019GL084192

Mishra, V., Thirumalai, K., Singh, D., & Aadhar, S. (2020). Future exacerbation of hot and dry summer monsoon extremes in India. *Npj Climate and Atmospheric Science*, *3*(1), 1–9. https://doi.org/10.1038/s41612-020-0113-5

Mukherjee, A., Fryar, A. E., & Rowe, H. D. (2007). Regional-scale stable isotopic signatures of recharge and deep groundwater in the arsenic affected areas of West Bengal, India. *Journal of Hydrology*, *334*(1–2), 151–161. https://doi.org/10.1016/j.jhydrol.2006.10.004

Nepal, S., Flügel, W.-A., & Shrestha, A. B. (2014). Upstream-downstream linkages of hydrological processes in the Himalayan region. *Ecological Processes*, *3*(1), 19. https://doi.org/10.1186/s13717-014-0019-4

Pfahl, S., & Sodemann, H. (2014). What controls deuterium excess in global precipitation? *Climate of the Past*, *10*(2), 771–781. https://doi.org/10.5194/cp-10-771-2014

Pokharel, B., Wang, S. Y. S., Meyer, J., Marahatta, S., Nepal, B., Chikamoto, Y., & Gillies, R. (2020). The east–west division of changing precipitation in Nepal. *International Journal of Climatology*, *40*(7), 3348–3359. https://doi.org/10.1002/joc.6401

Rowley, D. B., Pierrehumbert, R. T., & Currie, B. S. (2001). A new approach to stable isotope-based paleoaltimetry: Implications for paleoaltimetry and paleohypsometry of the High Himalaya since the Late Miocene. *Earth and Planetary Science Letters*, *188*(1–2), 253–268. https://doi.org/10.1016/S0012-821X(01)00324-7

Sharp, Z. D. (2017). Principles of stable isotope geochemistry (2nd ed.). https://doi.org/10.25844/h9q1-0p82

Stein, A. F., Draxler, R. R., Rolph, G. D., Stunder, B. J. B., Cohen, M. D., & Ngan, F. (2015). NOAA's HYSPLIT atmospheric transport and dispersion modeling system. *Bulletin of the American Meteorological Society*, *96*(12), 2059–2077. https://doi.org/10.1175/BAMS-D-14-00110.1

Stewart, M. K. (1975). Stable isotope fractionation due to evaporation and isotopic exchange of falling waterdrops: Applications to atmospheric processes and evaporation of lakes. *Journal of Geophysical Research*, *80*(9), 1133–1146. https://doi.org/10.1029/JC080i009p01133

Struck, M., Andermann, C., Hovius, N., Korup, O., Turowski, J. M., Bista, R., et al. (2015). Monsoonal hillslope processes determine grain size-specific suspended sediment fluxes in a trans-Himalayan river. *Geophysical Research Letters*, *42*(7), 2302–2308. https://doi.org/10.1002/2015GL063360

Taft, L., Wiechert, U., Riedel, F., Weynell, M., & Zhang, H. (2012). Sub-seasonal oxygen and carbon isotope variations in shells of modern *Radix* sp. (Gastropoda) from the Tibetan Plateau: Potential of a new archive for palaeoclimatic studies. *Quaternary Science Reviews*, *34*, 44–56. https://doi.org/10.1016/j.quascirev.2011.12.006

Talchabhadel, R., Panthi, J., Sharma, S., Ghimire, G. R., Baniya, R., Dahal, P., et al. (2021). Insights on the impacts of hydroclimatic extremes and anthropogenic activities on sediment yield of a river basin. *Earth*, *2*(1), 32–50. https://doi.org/10.3390/earth2010003

Tuinenburg, O. A., Hutjes, R. W. A., & Kabat, P. (2012). The fate of evaporated water from the Ganges basin. *Journal of Geophysical Research*, *117*(1), 1–17. https://doi.org/10.1029/2011JD016221

Wang, D., Tian, L., Cai, Z., Shao, L., Guo, X., Tian, R., et al. (2020). Indian monsoon precipitation isotopes linked with high level cloud cover at local and regional scales. *Earth and Planetary Science Letters*, *529*, 115837. https://doi.org/10.1016/j.epsl.2019.115837

Warner, M. S. C. (2018). Introduction to PySPLIT: A Python toolkit for NOAA ARL's HYSPLIT model. *Computing in Science and Engineering*, *20*(5), 47–62. https://doi.org/10.1109/MCSE.2017.3301549

Wilson, A. M., Williams, M. W., Kayastha, R. B., & Racoviteanu, A. (2015). Use of a hydrologic mixing model to examine the roles of meltwater, precipitation and groundwater in the Langtang River basin, Nepal. *Annals of Glaciology*, *57*(71), 155–168. https://doi.org/10.3189/2016AoG71A067

Winnick, M. J., Chamberlain, C. P., Caves, J. K., & Welker, J. M. (2014). Quantifying the isotopic "continental effect". *Earth and Planetary Science Letters*, *406*, 123–133. https://doi.org/10.1016/J.EPSL.2014.09.005

Wolf, A., Roberts, W. H. G., Ersek, V., Johnson, K. R., & Griffiths, M. L. (2020). Rainwater isotopes in central Vietnam controlled by two oceanic moisture sources and rainout effects. *Scientific Reports*, *10*(1), 1–14. https://doi.org/10.1038/s41598-020-73508-z

Wulf, H., Bookhagen, B., & Scherler, D. (2016). Differentiating between rain, snow, and glacier contributions to river discharge in the Western Himalaya using remote-sensing data and distributed hydrological modeling. *Advances in Water Resources*, *88*, 152–169. https://doi.org/10.1016/j.advwatres.2015.12.004

Yao, T., Masson-Delmotte, V., Gao, J., Yu, W., Yang, X., Risi, C., et al. (2013). A review of climatic controls on $\delta^{18}O$ in precipitation over the Tibetan Plateau: Observations and simulations. *Reviews of Geophysics*, *51*(4), 525–548. https://doi.org/10.1002/rog.20023

Zängl, G., Egger, J., & Wirth, V. (2001). Diurnal winds in the Himalayan Kali Gandaki valley. Part II: Modeling. *Monthly Weather Review*, *129*(5), 1062–1080. https://doi.org/10.1175/1520-0493(2001)129<1062:DWITHK>2.0.CO;2

References From the Supporting Information

Dee, S., Noone, D., Buenning, N., Emile-Geay, J., & Zhou, Y. (2015). SPEEDY-IER: A fast atmospheric GCM with water isotope physics. *Journal of Geophysical Research*, *120*(1), 73–91. https://doi.org/10.1002/2014JD022194

Gibson, J. J., Birks, S. J., & Yi, Y. (2016). Stable isotope mass balance of lakes: A contemporary perspective. *Quaternary Science Reviews*, *131*, 316–328. https://doi.org/10.1016/j.quascirev.2015.04.013

IAEA/WMO. (2017). *Global network of isotopes in precipitation*. The GNIP Database. Retrieved from https://nucleus.iaea.org/wiser

Merlivat, L., & Nief, G. (1967). Fractionnement isotopique lors des changements d'état solide-vapeur et liquide-vapeur de l'eau Á des températures inférieures Á 0°C. *Tellus*, *19*(1), 122–127. https://doi.org/10.3402/tellusa.v19i1.9756

Nusbaumer, J., Wong, T. E., Bardeen, C., & Noone, D. (2017). Evaluating hydrological processes in the Community Atmosphere Model Version 5 (CAM5) using stable isotope ratios of water. *Journal of Advances in Modeling Earth Systems*, *9*, 949–977. https://doi.org/10.1002/2016MS000839

Sodemann, H., Schwierz, C., & Wernli, H. (2008). Interannual variability of Greenland winter precipitation sources: Lagrangian moisture diagnostic and North Atlantic Oscillation influence. *Journal of Geophysical Research*, *113*(3), 1–17. https://doi.org/10.1029/2007JD008503

Werner, M., Langebroek, P. M., Carlsen, T., Herold, M., & Lohmann, G. (2011). Stable water isotopes in the ECHAM5 general circulation model: Toward high-resolution isotope modeling on a global scale. *Journal of Geophysical Research*, *116*(D15), D15109. https://doi.org/10.1029/2011JD015681

Wong, T. E., Nusbaumer, J., & Noone, D. C. (2017). Evaluation of modeled land-atmosphere exchanges with a comprehensive water isotope fractionation scheme in version 4 of the Community Land Model. *Journal of Advances in Modeling Earth Systems*, *9*(2), 978–1001. https://doi.org/10.1002/2016MS000842